CRREL
REPORT 84-2

US Army Corps
of Engineers
Cold Regions Research &
Engineering Laboratory

Electromagnetic properties of sea ice

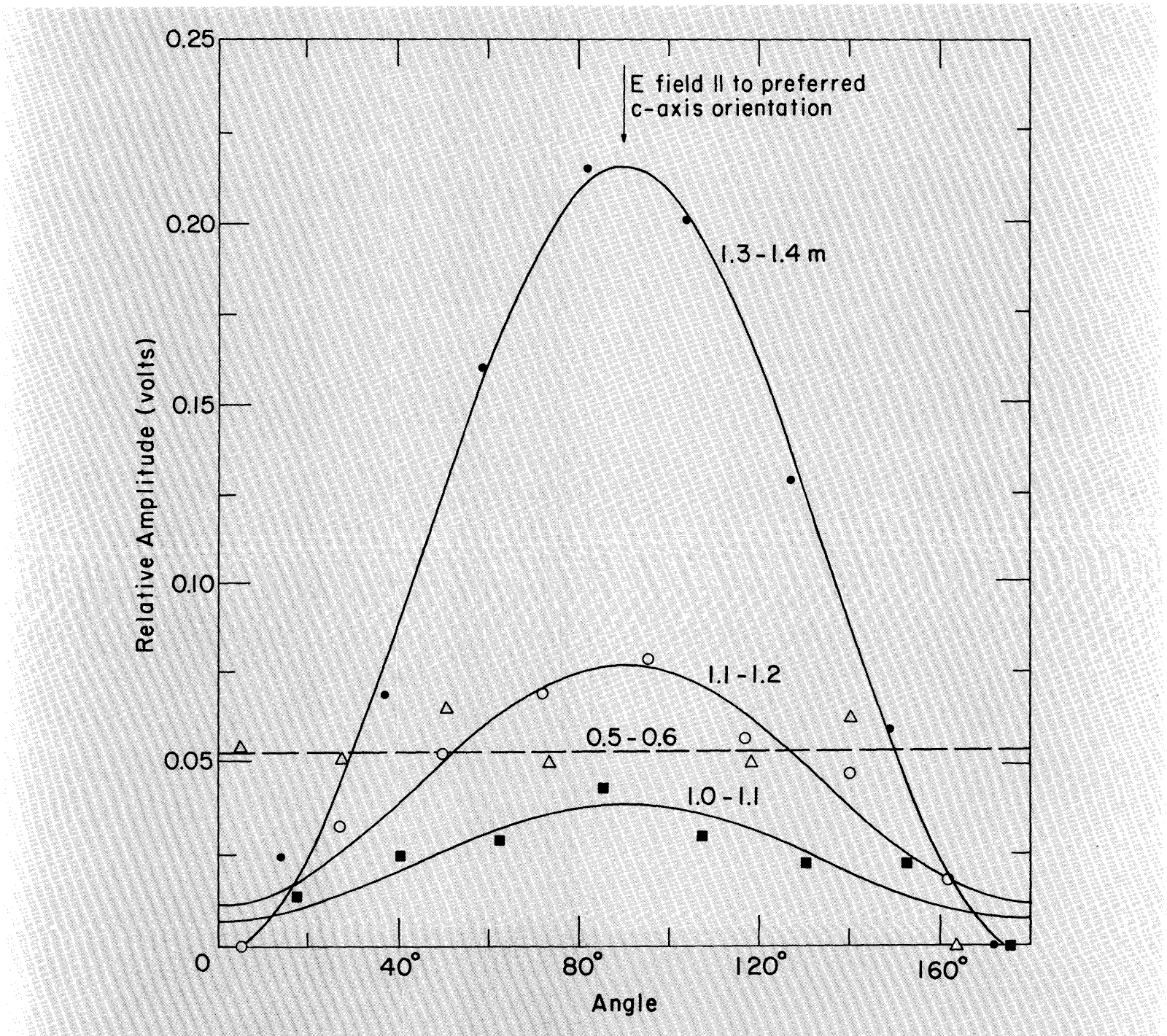

CRREL Report 84-2

January 1984

Electromagnetic properties of sea ice

R.M. Morey, A. Kovacs and G.F.N. Cox

Prepared for
OFFICE OF THE CHIEF OF ENGINEERS

REPORT DOCUMENTATION PAGE

READ INSTRUCTIONS BEFORE COMPLETING FORM

1. REPORT NUMBER: CRREL Report 84-2	2. GOVT ACCESSION NO.
3. RECIPIENT'S CATALOG NUMBER	
4. TITLE *(and Subtitle)*: ELECTROMAGNETIC PROPERTIES OF SEA ICE	5. TYPE OF REPORT & PERIOD COVERED
	6. PERFORMING ORG. REPORT NUMBER
7. AUTHOR*(s)*: R.M. Morey, A. Kovacs and G.F.N. Cox	8. CONTRACT OR GRANT NUMBER*(s)*: Contract DE-AI21-83MC20022
9. PERFORMING ORGANIZATION NAME AND ADDRESS: U.S. Army Cold Regions Research and Engineering Laboratory, Hanover, New Hampshire 03755	10. PROGRAM ELEMENT, PROJECT, TASK AREA & WORK UNIT NUMBERS
11. CONTROLLING OFFICE NAME AND ADDRESS: Department of Energy, Morgantown, West Virginia 26505	12. REPORT DATE: January 1984
	13. NUMBER OF PAGES: 38
14. MONITORING AGENCY NAME & ADDRESS*(if different from Controlling Office)*	15. SECURITY CLASS. *(of this report)*: Unclassified
	15a. DECLASSIFICATION/DOWNGRADING SCHEDULE

16. DISTRIBUTION STATEMENT *(of this Report)*

Approved for public release; distribution unlimited.

17. DISTRIBUTION STATEMENT *(of the abstract entered in Block 20, if different from Report)*

18. SUPPLEMENTARY NOTES

19. KEY WORDS *(Continue on reverse side if necessary and identify by block number)*

Conductivity
Dielectric constants
Electromagnetic propagation
Sea ice
Time domain spectroscopy

20. ABSTRACT *(Continue on reverse side if necessary and identify by block number)*

Investigations of the in situ complex dielectric constant of sea ice were made using time-domain spectroscopy. It was found that (1) for sea ice with a preferred horizontal crystal c-axis alignment, the anisotropy or polarizing properties of the ice increased with depth, (2) brine inclusion conductivity increased with decreasing temperature down to about -8°C, at which point the conductivity decreased with decreasing temperature, (3) the DC conductivity of sea ice increased with increasing brine volume, (4) the real part of the complex dielectric constant is strongly dependent upon brine volume but less dependent upon the brine inclusion orientation, (5) the imaginary part of the complex dielectric constant was strongly dependent upon brine inclusion orientation but much less dependent upon brine volume. Because the electromagnetic (EM) properties of sea ice are dependent upon the physical state of the

ice, which is continually changing, it appears that only trends in the relationships between the EM properties of natural sea ice and its brine volume and brine inclusion microstructure can be established.

PREFACE

This report was prepared by Austin Kovacs, Research Civil Engineer of the Applied Research Branch, Experimental Engineering Division; Gordon F.N. Cox, Research Geophysicist, of the Snow and Ice Branch, Research Division, U.S. Army Cold Regions Research and Engineering Laboratory, and Rexford M. Morey, Geophysical Systems Consultant, Nashua, N.H. Funding for this study was provided by the U.S. Department of Energy under Contract No. DE-AI21-83MC20022 and in part by the Bureau of Land Management through the National Oceanic and Atmospheric Administration's Alaska Outer Continental Shelf Environmental Assessment Program.

Dr. W.F. Weeks and D.L. Minsk provided useful counsel and technical review of this report.

The contents of this report are not to be used for advertising or promotional purposes. Citation of brand names does not constitute an official endorsement or approval of the use of such commercial products.

CONTENTS

ILLUSTRATIONS

Figure

TABLES

NOMENCLATURE

A	attenuation rate (dB/m)
A_r	relative attenuation
a	diameter
b	separation distance
c	velocity of light in a vacuum (3×10^8 m/s)
FF	formation factor
f	frequency (MHz)
ℓ	length; large dimension of ellipsoid
N	normality
n	depolarization factor
S	conductance (siemens)
s_b	salinity of brine ($^0/_{00}$)
T	temperature ($^\circ$C)
$T(j\omega)$	transmission coefficient
t	travel time (ns)
v	velocity of propagation
v_e	effective velocity of propagation
v_m	velocity of propagation in material
Z	impedance of transmission line
Z_c	characteristic impedance
α	attenuation constant
β	phase constant
γ	complex propagation constant
ϵ	dielectric constant
ϵ^*	complex dielectric constant
ϵ', ϵ''	real and imaginary parts of ϵ^*
ϵ_a	apparent dielectric constant
ϵ_e	effective dielectric constant
$\epsilon'_e, \epsilon''_e$	real and imaginary parts of ϵ_e
ϵ_{er}	effective relative dielectric constant
ϵ_o	free space dielectric constant
ϵ_r	relative dielectric constant
ϵ^*_r	relative complex dielectric constant
$\epsilon'_r, \epsilon''_r$	real and imaginary parts of ϵ^*_r
ϵ^*_{rb}	relative complex dielectric constant of brine
$\epsilon'_{rb}, \epsilon''_{rb}$	real and imaginary parts of ϵ^*_{rb}
ϵ_{rH}	relative dielectric constant of host (ice)
ϵ_{rI}	relative dielectric constant of inclusion (brine)
ϵ^*_{ri}	relative complex dielectric constant of ice
ϵ_{rm}	relative dielectric constant of mixture
ϵ^*_{rm}	relative complex dielectric constant of mixture
$\epsilon'_{rm}, \epsilon''_{rm}$	real and imaginary parts of ϵ^*_{rm}
ϵ_{rs}	relative static dielectric constant
ϵ_{rsb}	relative static dielectric constant of brine
ϵ^*_{rw}	relative complex dielectric constant of sea water
$\epsilon_{r\infty}$	relative optical or high-frequency dielectric constant
ζ	volume fraction of inclusions
η_2	intrinsic complex impedance
λ	wavelength
μ^*	complex magnetic permeability
μ', μ''	real and imaginary parts of μ^*
υ	brine volume of ice ($^0/_{00}$)
ρ	coefficient of reflection
ρ_o	low-frequency coefficient of reflection
σ^*	complex conductivity
σ', σ''	real and imaginary parts of σ^*
σ_{DC}	DC conductivity (S/m)
σ_{si}	conductivity of sea ice
σ_b	conductivity of brine
σ_{NaCl}	conductivity of NaCl solution (S/m)
τ	relaxation time (s)
τ_b	relaxation time of brine (s)
ϕ	porosity (%)
ω	angular frequency ($2\pi f$)

ELECTROMAGNETIC PROPERTIES OF SEA ICE

R.M. Morey, A. Kovacs and G.F.N. Cox

INTRODUCTION

Sea ice is a complex, lossy, anisotropic dielectric consisting of pure ice, liquid brine, and air (gas). One method for studying the properties and structure of sea ice is to probe the ice with electromagnetic (EM) energy, measuring parameters such as the amplitude and phase of the reflected energy and the attenuation and travel time of an EM wavelet through the ice. These measurements can be made remotely using radar techniques (Kovacs and Morey 1978, 1979, 1980) or on samples using transmission-line techniques (Vant et al. 1978).

Knowledge of the dielectric properties of sea ice forms the basis for measurement of its other properties, such as thickness and strength, using electromagnetic methods. The complex dielectric constant ϵ^* determines the velocity of the EM wavelet or signal propagation through the ice. Therefore, the transit time of a radar pulse to the bottom of the ice and back can be correlated to ice thickness. The ratio of the imaginary part of the dielectric constant ϵ'' to the real part ϵ' expresses the absorption of electromagnetic energy in the ice and thus the depth of penetration for any particular radar system.

Since first-year sea ice is dynamic, in the sense that it is either growing or decaying, the accurate measurement of its dielectric properties must account for this time-dependent characteristic. As an example, typical sampling methods require the removal of a piece of ice from the ice sheet. This process alters the sea ice sample, especially for ice near the bottom of the ice sheet where high porosity allows for rapid brine drainage and as a resultant change in ice properties. In other words, the mere process of extraction and measurement creates an "artificial" saline ice sample. Likewise, growing "sea ice" in the laboratory does not necessarily recreate ice that has the same dielectric properties as natural sea ice, especially in relation to crystal structure and brine inclusion geometry and spatial arrangement.

This report describes a variety of transmission line "cells" that were used to measure the dielectric properties of sea ice. Measurements were made in situ as well as on samples removed from the sea ice. Time-domain spectroscopy (TDS) methods were used to measure both the reflection (TDR) and transmission (TDT) characteristics of sea ice in the 100- to 300-MHz frequency range.

DIELECTRIC PROPERTIES OF SEA ICE

The complex dielectric constant of sea ice is not a unique function of the fractional volumes of the different phases present, but depends also on their geometric form and distribution. For example, when a layered structure is formed of parallel plates or quasi-plates that have alternating dielectric constants, the effective complex dielectric constant depends on the orientation of the plates to the electric field. When the electric (E) field is perpendicular to the layers, the complex dielectric constant is less than when the E field is parallel to them.

Propagation of electromagnetic energy in sea ice can be described by the complex propagation constant γ, which is defined (Kraichman 1976) as:

$$\gamma = \alpha + j\beta = (-\omega^2 \mu' \epsilon_e + j\omega\mu'\sigma_e)^{1/2} \tag{1}$$

where α = attenuation constant
β = phase constant
ω = angular frequency = $2\pi f$
f = frequency
μ' = real part of magnetic permeability
ϵ_e = effective dielectric constant
σ_e = effective conductivity
$j = \sqrt{-1}$.

As the electromagnetic wave propagates through the ice with a phase velocity

$$v_m = \omega/\beta \quad \text{(m/s)} \tag{2}$$

it suffers an exponential attenuation

$$A = 20 \log e^{\alpha} = 8.686\alpha \quad \text{(dB/m)} . \tag{3}$$

All materials are described by complex, media-dependent parameters defined as:

$\epsilon^* = \epsilon' - j\epsilon''$ = complex dielectric constant

$\sigma^* = \sigma' - j\sigma''$ = complex electrical conductivity

$\mu^* = \mu' - j\mu''$ = complex magnetic permeability

where ϵ', σ', and μ' are the real parts, and ϵ'', σ'', and μ'' are the imaginary parts, or loss factors.

The relative complex dielectric constant ϵ_r^* is related to ϵ^* by:

$$\epsilon^* = \epsilon_o \epsilon_r^* \tag{4}$$

where ϵ_o, the free-space dielectric constant, is

$$\epsilon_o = (1/36\pi) \times 10^{-9} \text{ F/m}$$

where F = farad. The magnetic permeability μ^* is assumed to be real for sea ice, such that $\mu^* = \mu'$ and the real relative permeability $\mu_r' = 1$.

The parameters ϵ_e and σ_e in eq 1 can be measured and are related to the complex constitutive parameters by:

$$\sigma_e = \sigma' + \omega\epsilon'' \quad \text{(S/m)} \tag{5}$$

$$\epsilon_e = \epsilon' - (\sigma''/\omega) \approx \epsilon' \quad \text{(F/m)} \tag{6}$$

where σ' equals the DC conductivity (σ_{DC}), σ'' equals zero at the frequencies of interest, and S is conductance in siemens. Electromagnetic energy is dissipated in ice in the form of heat; it is the sum of two energy dissipation processes, namely relaxation and conduction. The dielectric relaxation loss factor ϵ'' is due to the drag of dipolar water molecules oscillating in a time-varying electric field. Conduction is caused by electron and ion movement in an electric field. Water that contains free carriers in the form of dissolved salts increases the conductivity of sea ice. Therefore, the presence of water can contribute to both loss mechanisms. However, the dissipation processes are dominant in different portions of the electromagnetic frequency spectrum: conduction at low frequencies and relaxation at high frequencies. The imaginary effective dielectric constant is given by:

$$\epsilon_e'' = \epsilon'' + (\sigma'/\omega) = (\sigma_e/\omega).$$

The relative complex dielectric constant of sea water ϵ_r^* is frequency-, temperature-, and salinity-dependent. It is obtained from the Debye formula (Stogryn 1971),

$$\epsilon_r^* = \epsilon_r' - j\epsilon_r'' = \epsilon_{r\infty} + \frac{\epsilon_{rs} - \epsilon_{r\infty}}{1 + j\omega\tau} - j\,\frac{\sigma_{DC}}{\omega\epsilon_o} \tag{7}$$

where ϵ_r' = relative real dielectric constant
ϵ_r'' = relative imaginary dielectric constant
ϵ_{rs} = relative static dielectric constant (temperature- and salinity-dependent)
$\epsilon_{r\infty}$ = relative optical dielectric constant for sea water [$\epsilon_{r\infty} = 5.5$ (King and Smith 1981)]
τ = relaxation time (temperature- and salinity-dependent)
σ_{DC} = ionic conductivity of dissolved salts (S/m).

There are some limitations in applying Stogryn's analysis to sea ice. Several of his equations were derived from data on NaCl solutions and not on sea water. In addition, his analysis was based on data obtained at temperatures higher than 0°C. No dielectric data seems to be available on high salinity ($>50^0/_{00}$) sea water at low temperatures ($t < -5$°C). Therefore we will use some of the equations of Stogryn (1971) and Vant et al. (1978).

At 0°C and a frequency of 8.9×10^9 Hz, the relative static dielectric constant ϵ_{rs} and the relaxation time τ for water are respectively 88.2 and 17.8×10^{-12} s. For pure ice at 0°C and a frequency of 7.76×10^3 Hz, $\epsilon_{rs} = 91.1$ and $\tau = 2.05\times10^{-5}$ s. The relative static dielectric constant of ice and water as a function of temperature is shown in Figure 1, and the relaxation time for pure ice and water as a function of temperature is shown in Figure 2. The Debye equation for determining the relative complex dielectric constant ϵ_r^* for pure ice is

$$\epsilon_r^* = \epsilon_r' - j\epsilon_r'' = 3.14 + \frac{\epsilon_{rs} - 3.14}{1 + j\omega\tau}\,. \tag{8}$$

The losses due to the relaxation process in sea ice occur at extremely high frequencies, $>10^9$ Hz, and are only dependent on the water content.

The effective conductivity of sea ice is fairly independent of frequency from 0 to about 10 MHz, indicating that σ' in eq 5 is the dominant factor in determining the propagation losses in sea ice at low frequencies. For sea ice with no free water, σ_e equals the DC conductivity and is independent of frequency because ϵ'' is zero. In addition, if the brine volume of sea ice is known, ϵ_e can be estimated from a dielectric mixing model that will be discussed later.

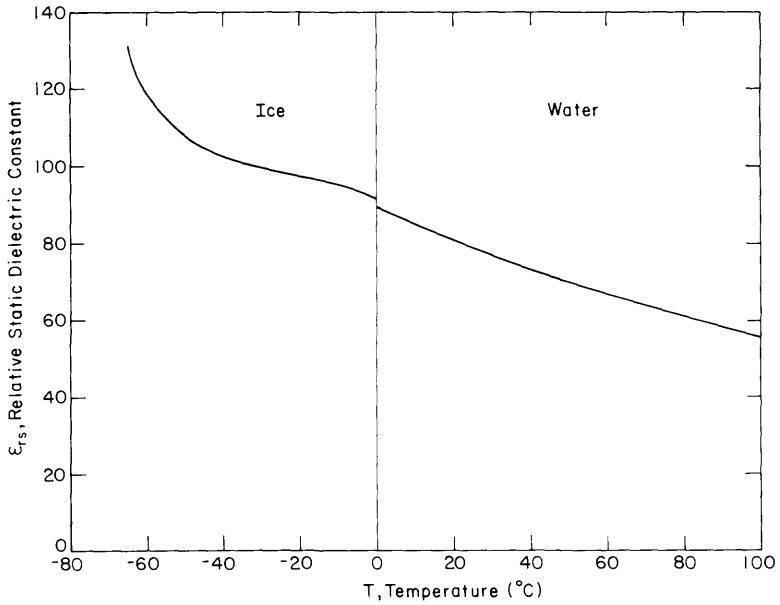

Figure 1. Relative static dielectric constant of ice and water as a function of temperature (after King and Smith 1981).

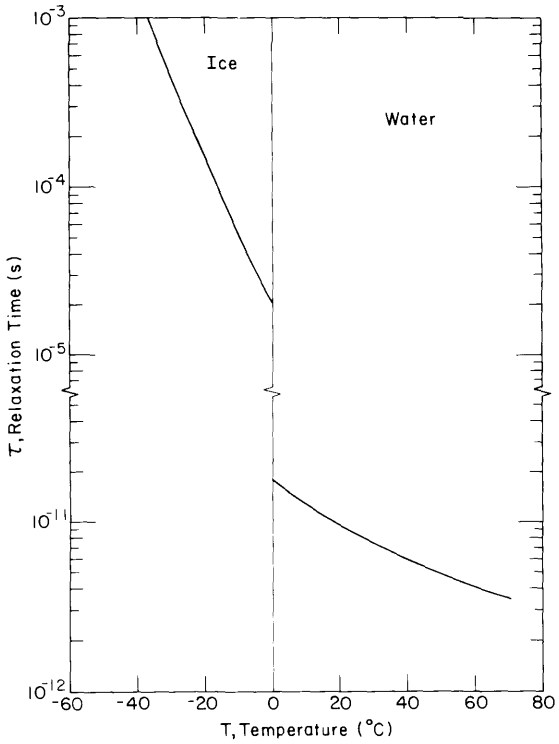

Figure 2. Relaxation time of pure ice and water as a function of temperature (after King and Smith 1981).

Since the submerged portion of sea ice is a "saturated" mixture of brine pockets in an ice matrix, where the brine pockets contain salt and liquid water, the ratio of brine to ice should determine the complex dielectric constant of the sea ice. However, field observations (e.g. Peyton 1966; Cherepanov 1973; Kovacs and Morey 1978; Weeks and Gow 1978, 1979) have shown that sea ice is anisotropic; the crystal structure varies in size and orientation with depth. Below 20 to 50 cm the crystals are composed of parallel platelets of pure ice with preferred horizontal *c*-axes. The *c*-axes frequently have a preferred azimuthal alignment that is parallel to the current existing at the ice/water interface at the time of ice crystal platelet growth. The brine pockets that exist between the fresh ice platelets are frequently described as ellipsoids, but in fact also have rather complex geometries. These pockets form an ordered array along the platelet boundaries, as depicted in Figure 3. Drainage routes, called brine feeder channels, form near the bottom of the ice sheet and radiate outward like the limbs of a tree from larger vertical drainage channels or tubes (Fig. 3b). The

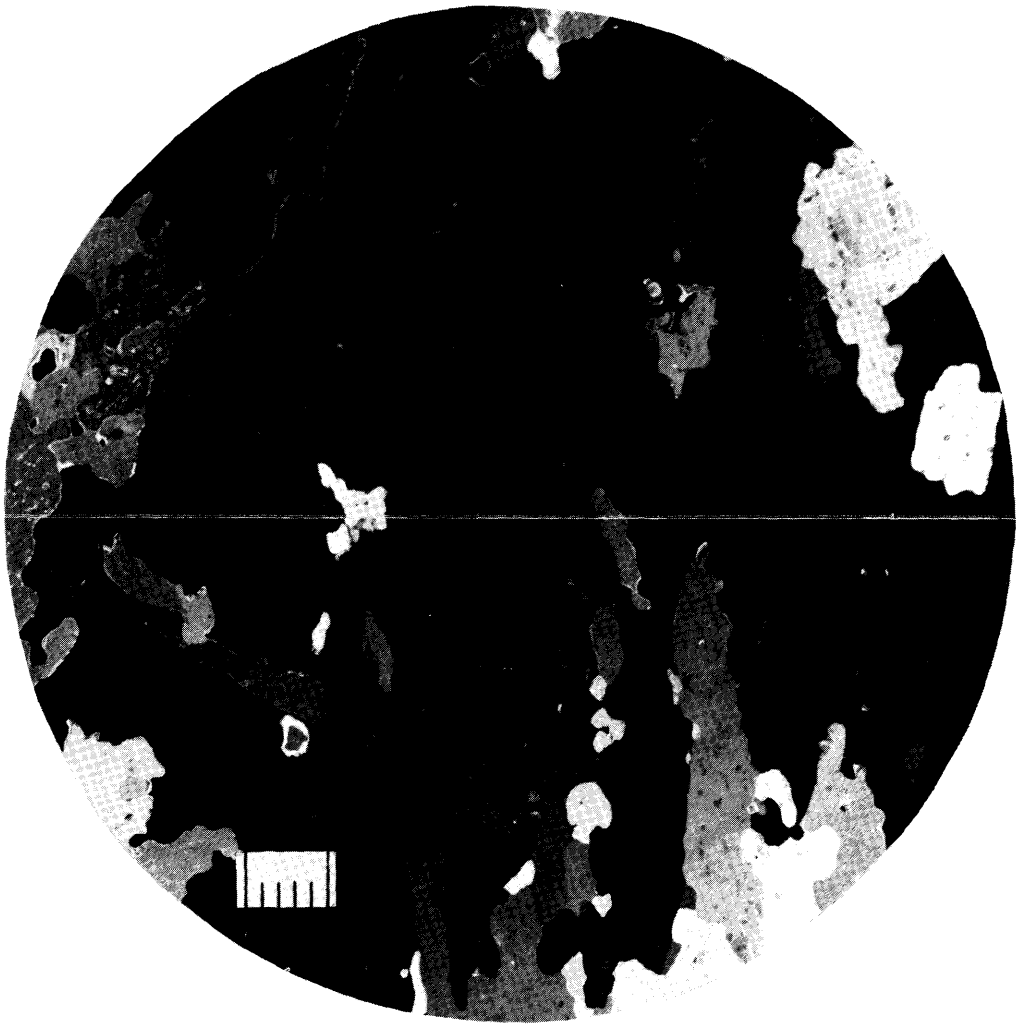

a. Thin section giving a vertical view of the individual ice crystals, the fresh ice platelets within each crystal, and the brine pockets scattered along the platelet boundary. Bar scale is in mm. Center line is preferred c-axis direction.

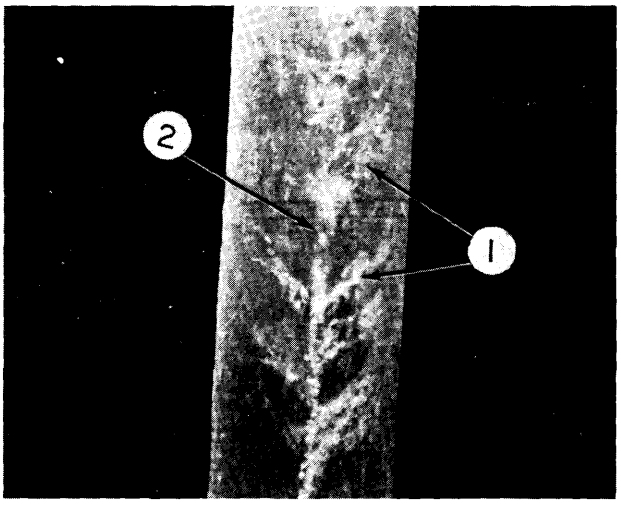

b. ,Vertical sea ice core showing relative configuration of brine drainage feeder channels (1) extending outward at ≈45° from the brine drainage tube (2). The tube extends vertically along the surface of the ice core.

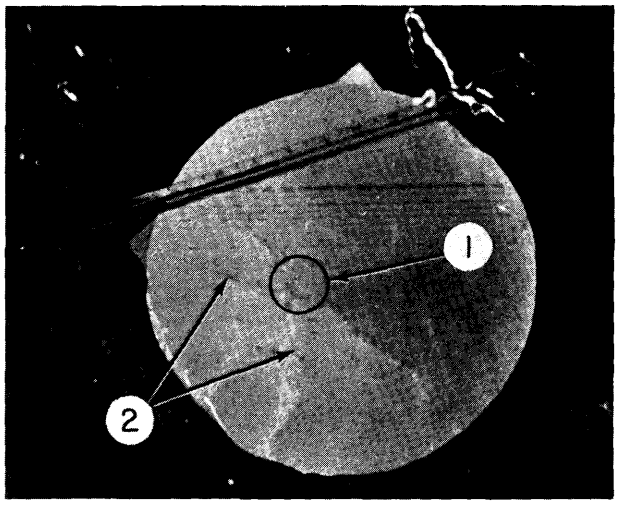

c. Horizontal section across a brine drainage tube. Radiating out from the central brine drainage tube area (1) are numerous brine drainage feeder channels (2).

Figure 3. Sea ice sections.

drainage tubes extend to the bottom of the sea ice. We have found these tubes spaced from 5 to 17 cm apart, but they are most often about 10 cm apart. Brine feeder channels are ribbon-like features, thin in the horizontal plane, that slope upward at an angle of 30° to 60° but on average are at about 45° (Niedrauer and Martin 1979). The channels that intercept the brine pockets near the ice bottom are the largest and give the ice a high porosity at the bottom and provide a route for brine drainage to the sea. The channels higher up in the ice sheet (channels left behind as the ice sheet grew thicker) become smaller with time.

To demonstrate the effect of the brine ellipsoidal inclusions, with preferred alignment between the ice crystal platelets on the dielectric properties of a host material, a simple model is assumed using the mixture formulas of Taylor (1965). Taylor's analysis assumes that the large dimension ℓ of the ellipsoid is much smaller than the wavelength λ of the signal. (λ_0 = 1 m at 300 MHz and ℓ is on the order of 0.3 mm for a brine pocket.) In addition to this assumption, the volume fraction of the inclusions is assumed to be much less than one. Using Taylor's notation, the normalized dielectric constant for a mixture containing needles with the major axis parallel to the electric field is

$$(\epsilon_{rm}/\epsilon_{rH})_{\parallel} = 1 - \zeta(1-\epsilon_{rI}/\epsilon_{rH}) \tag{9}$$

and for needles with the major axis perpendicular to the electric field is

$$(\epsilon_{rm}/\epsilon_{rH})_{\perp} = 1-2\zeta\,[1-(\epsilon_{rI}/\epsilon_{rH})]\;\frac{(\epsilon_{rm}/\epsilon_{rH})}{(\epsilon_{rm}/\epsilon_{rH})+(\epsilon_{rI}/\epsilon_{rH})} \tag{10}$$

where ϵ_{rm} = relative dielectric constant of the mixture
ϵ_{rH} = relative dielectric constant of the host (ice)
ϵ_{rI} = relative dielectric constant of the inclusions (brine)
$\zeta = V_I/V$ = volume fraction of the inclusions.

Equations 9 and 10 are valid when the inclusions and the host medium have zero conductivity, which is not the case for sea ice. However, it is instructive to plot ϵ_{rm} vs volume concentration for $\epsilon_{rH} \approx 3.2$ and $\epsilon_{rI} \approx 80$, as in Figure 4. If the effect of brine conductivity is included, there will be a slight increase in ϵ'_{rm} and a very large increase in the imaginary part, ϵ''_{rm}. In other words, for small volume concentrations the ϵ_{rm} calculations in Figure 4 would not change if brine conductivity were included. The curves in Figure 4 indicate that, even for small-inclusion volume concentrations (ζ = 0.1), there is a large difference (3 to 1) in the dielectric constants for parallel vs perpendicular polarization.

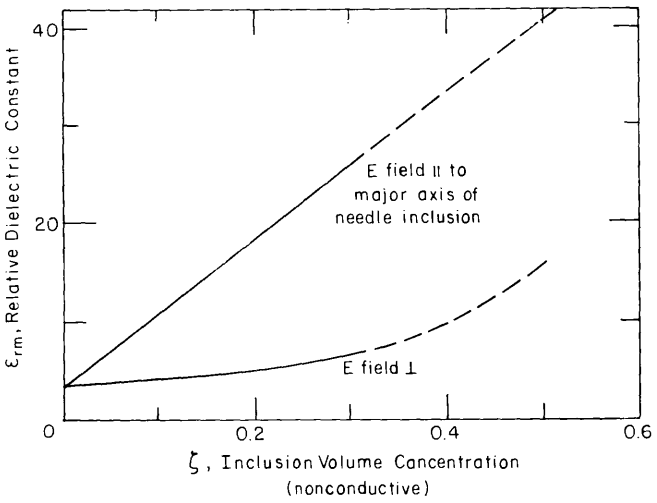

Figure 4. Relative real dielectric constant of sea ice-brine mixture as a function of inclusion volume concentration for the electric field parallel (∥) and perpendicular (⊥) to the major axis of the needle inclusions.

TIME-DOMAIN SPECTROSCOPY (TDS) MEASUREMENT

A time-domain reflectometer consists of a pulse generator that produces a fast-rise time step, a sampler that transforms a high-frequency signal into a lower frequency output, an oscilloscope, and a recording device (Fellner-Feldegg 1972, van Gemert 1973). With TDS techniques, the reflection coefficient at a discontinuity in a transmission line can be measured as well as the transmission coefficient through the sample. For a nonconductive dielectric, reflection coefficient ρ is a function of ϵ'

$$\rho = \frac{1-\sqrt{\epsilon'}}{1+\sqrt{\epsilon'}} \tag{11}$$

and

$$\epsilon' = \left(\frac{1-\rho}{1+\rho}\right)^2 . \tag{12}$$

The velocity of propagation v of the fast-rise time step is determined by the time t required to travel a known length L of the transmission line and is given by:

$$v \approx (L/t). \tag{13}$$

If a non-magnetic dielectric material is inserted in the transmission line, the propagation velocity v_m in the material is

$$v_m \approx (c/\sqrt{\epsilon_a}) \tag{14}$$

where ϵ_a is the apparent measured dielectric constant of the material, and c is the velocity of light in vacuum (3×10^8 m/s). The apparent dielectric constant is

$$\epsilon_a = \epsilon' \frac{1+\sqrt{1+\tan^2\delta}}{2} \tag{15}$$

where the loss tangent is

$$\tan\delta = \frac{\epsilon'' + (\sigma'/\omega\epsilon_o)}{\epsilon'} .$$

In low-loss materials ($\tan\delta \ll 1$),

$$\epsilon_a \simeq \epsilon' .$$

If the transmission line were inserted into the dielectric material, then we can combine eqs 13 and 14, yielding

$$\epsilon_a = (ct/L)^2 . \tag{16}$$

In general, TDS measurements are made using a coaxial transmission line filled with a dielectric sample of known length. However, because of the nature of sea ice and our sampling capabilities, a variety of transmission line configurations was used. Figure 5 shows several possible conductor cross sections (Wheeler 1980). The characteristic impedance Z_o, for an empty, air-filled transmission line is a function of the cross section of the transmission line (Fig. 5). When low-loss dielectrics are

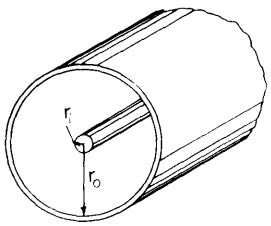

Coaxial

a. $Z_o = 60\ ln(r_o/r_i)$.

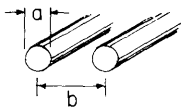

Two-conductor

b. $Z_o = 120\ \cosh^{-1}(b/a)$.

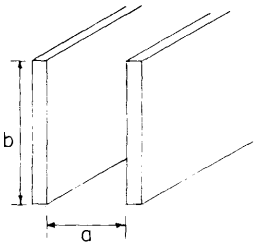

Parallel Plate

c. $Z_o \doteq 120\pi(a/b)$ *for* $a \ll b$.

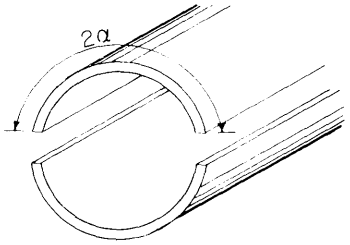

Quadrant Arc

d. $Z \doteq 30\ ln2(1+\sqrt{\cos\alpha})/(1-\sqrt{\cos\alpha})$ *for* $\alpha < 45°$.

Figure 5. Transmission line conductors of various cross sections.

inserted in or around the conductors, the transmission line impedance Z becomes

$$Z = (Z_o/\sqrt{\epsilon_a}). \tag{17}$$

and

$$\rho = \frac{Z-Z_o}{Z+Z_o}. \tag{18}$$

If there is an air gap between the conductor and the sample material, an error is introduced in the calculation of the apparent dielectric constant from eqs 16 or 17.

Laboratory measurements

To test the concept of measuring samples of anisotropic dielectrics, an artificial anisotropic dielectric block was made. Slabs of paraffin 10 cm square by 6 mm thick were interleaved with 10-cm-square pieces of filter paper to form a cube 10 cm on a side. Figure 6 shows one such cube. A parallel plate cell (Fig. 5c) was constructed to fit over the paraffin block (Fig. 7). Time-domain reflection (TDR) measurements were made with the electric field perpendicular (as in Fig. 7) and parallel to the layers of paraffin and paper. There was no measurable difference in the impedance between the two polarizations: the cell impedance was approximately 78 ohms and $\epsilon_a = 1.4$. Next, the block was put in a dish with 2.5 cm of saline water for several minutes so that the lower section of filter paper could absorb the salt water. The TDR measurements were repeated. The results are shown in Figure 8.

The input impedance of the empty cell was approximately 93 ohms. The impedance continues to increase along the length of the cell because some energy was radiated since the inequality in Figure 5c of $a \ll b$ was not maintained; in our cell $a \approx b$. The cell impedance with the electric field perpendicular to the brine-infiltrated paper was again about 78 ohms, and $\epsilon_a = 1.4$. The most striking change occurred when the electric field was parallel to the moist paper. The apparent dielectric constant was about 2 in the upper portion of the cell and about 3.5 in the lower section of the cell, implying a saline water volume concentration of about 0.1 (see Fig. 4) in the lower

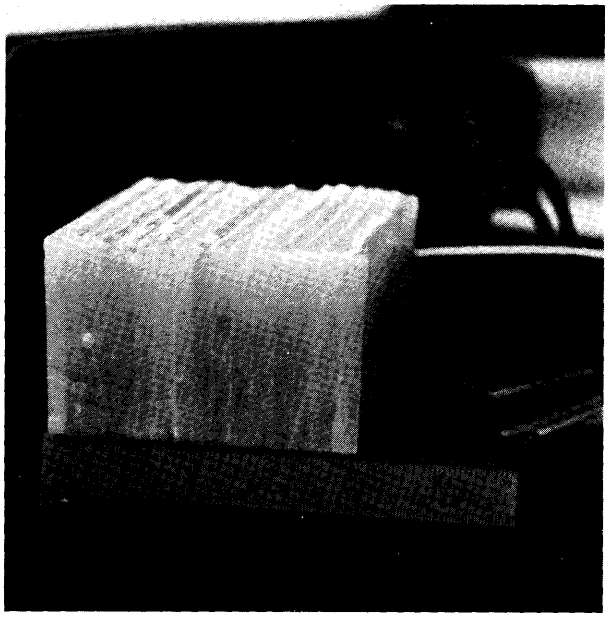

Figure 6. Artificial anisotropic dielectric block made of paraffin and filter paper.

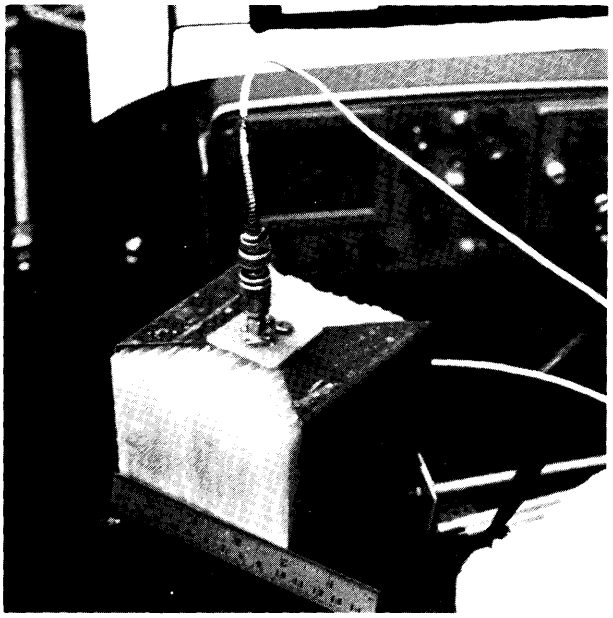

Figure 7. Parallel plate cell for measuring the anisotropy of dielectric blocks.

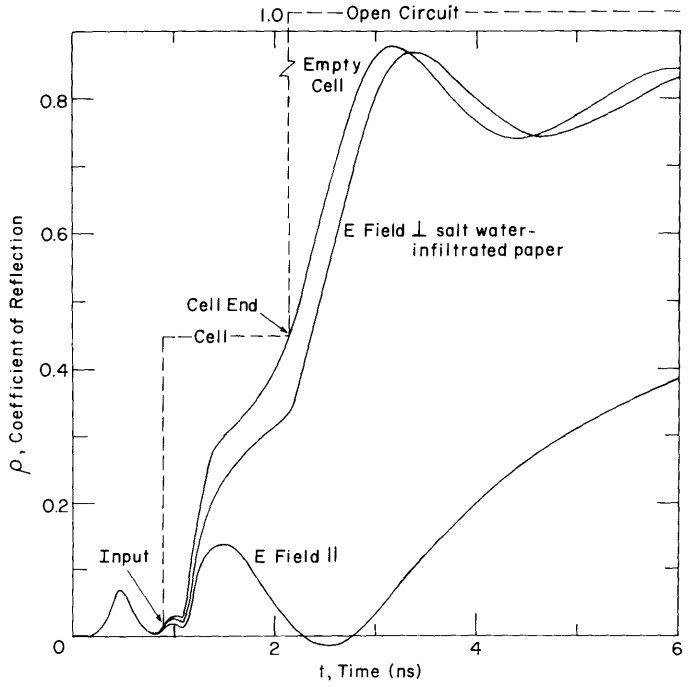

Figure 8. TDR plot of empty cell and cell with paraffin/filter paper block for two polarizations. The data do not follow the ideal response (dashed line) because it is not possible to generate a zero rise time step function and our cell geometry did not meet the criteria in Figure 5c.

section of the block where the filter paper was more saturated. Figure 8 also indicates that the signal is strongly attenuated when the electric field is parallel to the brine-infiltrated paper layers. A similar effect occurs in the strength of the reflected radar EM wavelet from the bottom of anisotropic sea ice when the electric field is parallel to the brine pockets, which are aligned along the ice

crystal platelet boundaries (Kovacs and Morey 1978, 1979, 1980). One reason for testing the parallel plate cell was to model the structure of the crystal platelets and brine pockets at the bottom of sea ice that has crystals with a preferred *c*-axis orientation; the cell could then be used in the field to measure the anisotropy of sea ice samples in situ. The idea was to cut two narrow slots 10 cm apart in the ice and slip the cell into the slots. Then the ice would be removed and the measurement repeated deeper into the ice sheet. As will be shown later, a more practicable cell design was used.

A two-conductor transmission line was also tested (Fig. 5b). Two metal rods 20 cm long and 6.4 mm in diameter were maintained parallel to each other with a center-to-center spacing of 1.04 cm. Two parallel holes were drilled into an 8-cm-diameter fresh ice core, and the metal rods were inserted. TDR measurements were made with the rods in air and in the fresh ice. The calculated impedance of the two-conductor transmission line (Fig. 5b) was 128.6 ohm, and the measured impedance, as determined from ρ, was 117.8 ohm. (The difference in these two values is probably due to the resolution of the measuring system.) The measured impedance of the line in ice was 64.68 ohm. Using eq 17 the apparent dielectric constant for the fresh ice was 3.36. Using eq 16 and the travel time along the 20-cm rods, the calculated apparent dielectric constant was 2.87. Published values of ϵ' for pure ice vary from about 2.9 to 3.2. In this report we use a value of 3.14, which is a good statistical average. The difference in ϵ' obtained from the TDR measurements and the value of 3.14 was probably due to a small air gap around the rods. Fresh water was poured on top of the ice core and allowed to trickle down and freeze around the rods to reduce any air gaps.

The subsequent TDR travel time measurement produced an $\epsilon_a = 3.07$, which is closer to the above value of 3.14. From our TDR results, the travel-time data seems to provide a better estimate of the apparent dielectric constant than the coefficient of reflection data.

Field measurements

TDS measurements were made on sea ice in the spring of 1979 and 1980 in the area of Prudhoe Bay, Alaska. The first measurements in 1979 were made near Exxon's experimental ice island, located a few kilometers north of Prudhoe Bay. The goal was to make TDR measurements in ice blocks as soon as the ice was excavated. Blocks of ice about 50 cm on a side were cut out with a chain saw. Each block was then laid on its side and two parallel holes, 6.4 mm in diameter, were drilled into the ice about 20 cm deep. Two metal rods were inserted into the holes (Fig. 9) and a TDR measurement was then made. When the rods were removed, the ice temperature was measured and an 8-cm diameter ice core was taken around the two rod holes. The core was retained for a salinity measurement. From the salinity and temperature data, the brine volume v of the ice was calculated. TDR and temperature measurements were made about every 10 cm from the surface down to the bottom of the ice sheet. The apparent dielectric constant of the ice was calculated from the travel time along the known length of the transmission line. Figure 10 is a plot of ϵ_a and v vs depth. There is a striking correlation between the apparent dielectric constant and the brine volume. Both the dielectric constant data and the brine volume data indicate a discontinuity at a depth of 30 cm. Earlier in the season, the area around the Exxon ice island had been flooded with sea water to build a thicker ice cover for transporting heavy equipment. The discontinuity at 30 cm is probably due to this flooding and freezing activity.

A large block of ice approximately 2 m square and 1.7 m deep had been removed from the sea ice near Spy Island for a diving operation. About 24 hours after its removal, TDR and temperature measurements were made, and ice cores were obtained along the length of the block (Fig. 11) for salinity determinations. A plot of apparent dielectric constant and brine volume vs ice depth is shown in Figure 12. Again, the correlation between ϵ_a and v is very good. The shape of the curves in Figure 12 is different from those in Figure 10. This is because considerable brine drainage had occurred between the time the ice block was removed and the time the Spy Island measurements were made.

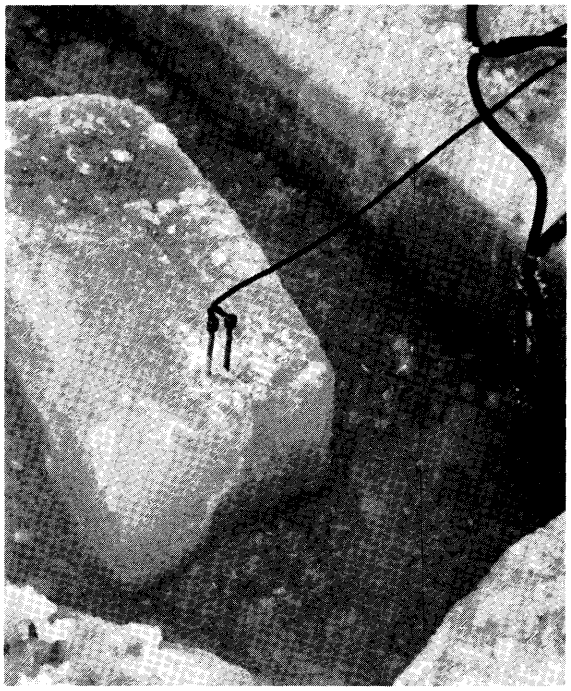

Figure 9. Two-conductor transmission lines in sea ice block. The block was from the bottom of the ice sheet. To prevent brine drainage and air cooling, the block was not removed from the sea water.

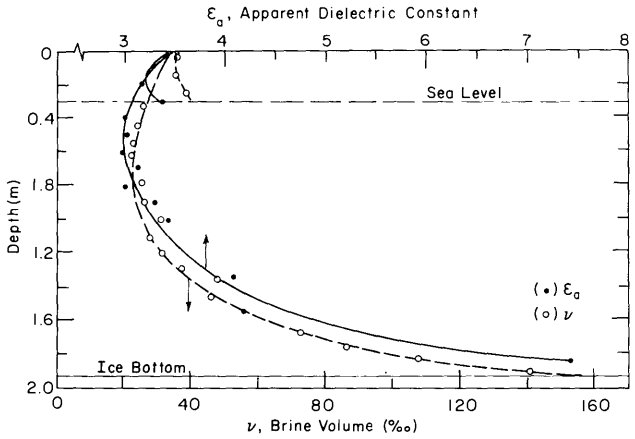

Figure 10. Apparent dielectric constant and brine volume as a function of depth at Exxon ice island site, 1979.

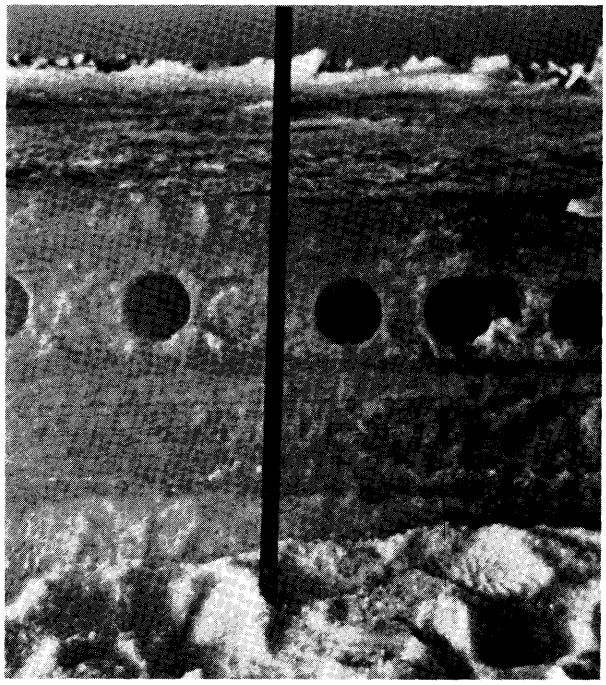

Figure 11. Photograph of sea ice block near Spy Island with cored holes.

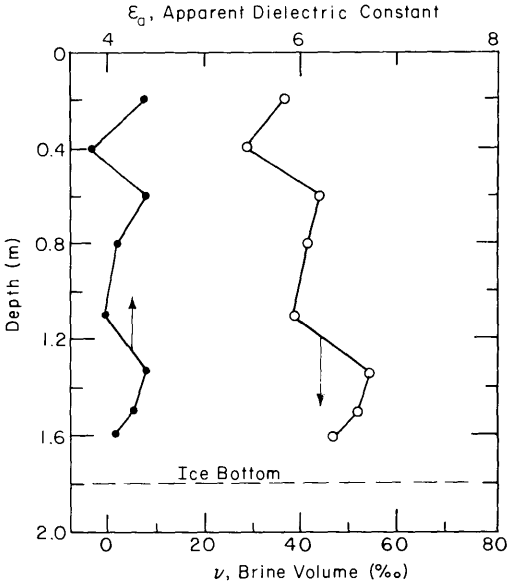

Figure 12. Apparent dielectric constant and brine volume as a function of depth at Spy Island site, 1979.

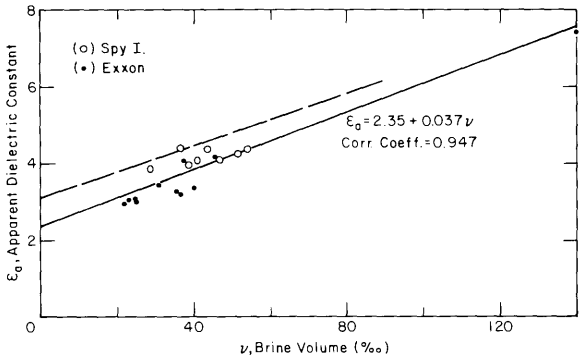

Figure 13. Apparent dielectric constant as a function of brine volume from the Exxon (1979) and Spy Island sites (1979).

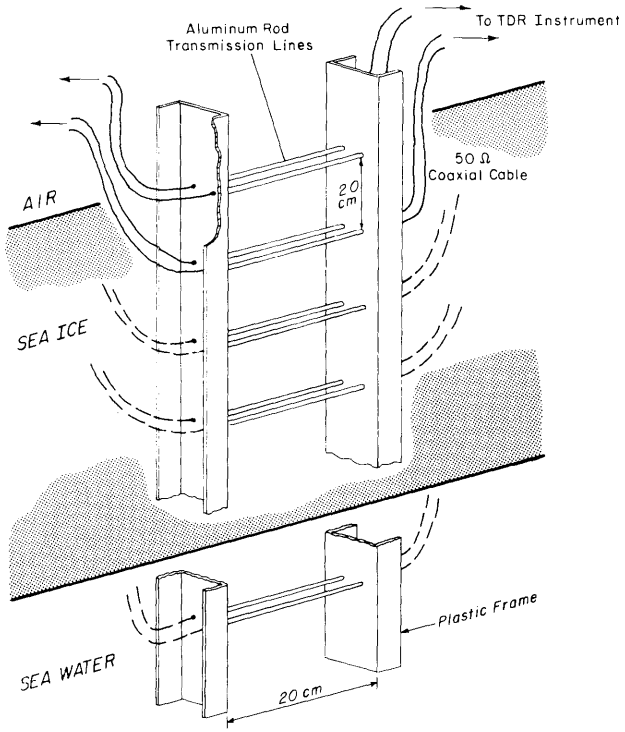

Figure 14. Schematic of ladder array of two-conductor transmission lines in sea ice.

A plot of brine volume vs apparent dielectric constant from the two sites is given in Figure 13. The dielectric values in Figure 13 are lower than the effective bulk dielectric constant values obtained by Kovacs and Morey (1980) using radar EM wavelet transmission time measurements as indicated by the dashed curve, which fits their data. The lower values obtained in this study may be due to a very small air gap around the rods or they may be caused by air pockets in the ice due to brine drainage. In any case, the two-conductor transmission line TDR measurement technique tends to give lower values of ϵ_a. For example, clear, bubble-free lake ice in the Prudhoe Bay area was measured using the two-conductor TDR

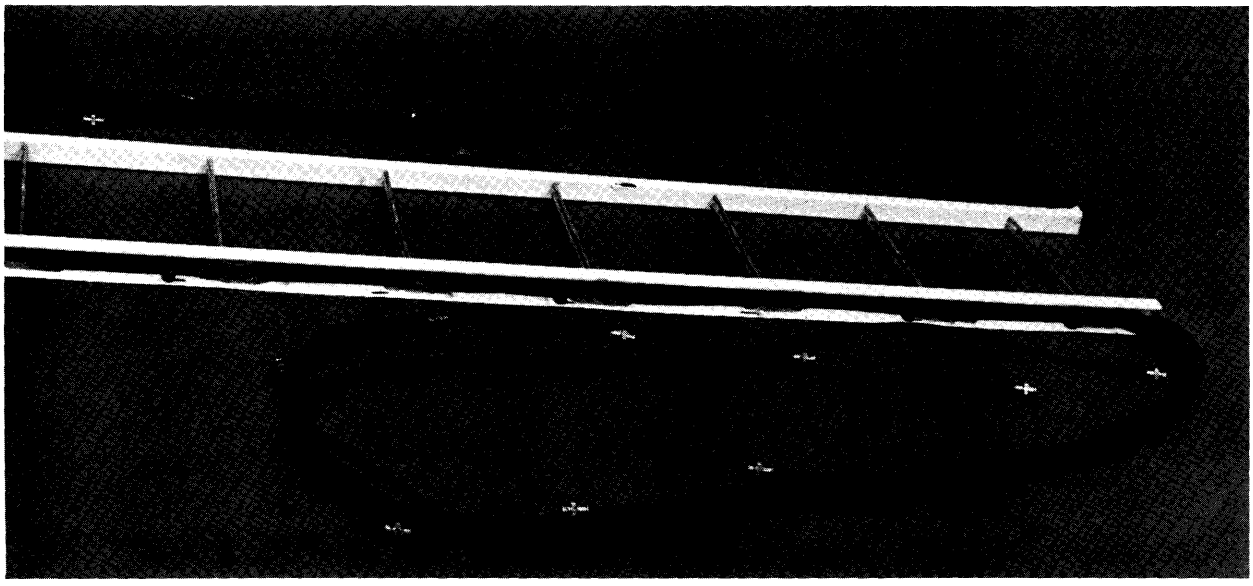

Figure 15. Ladder array of two-conductor transmission lines.

Figure 16. Coaxial cables and top of ladder array protruding from sea ice.

technique, and the apparent dielectric constant was found to be 2.72 instead of an expected value of ~3.14. Davis (1979), using similar dual-rod TDR techniques, also obtained low apparent dielectric constant values for ice.

Because the above measurements were made on sea ice that was disturbed and had experienced brine drainage, an experiment was devised in which the two-conductor transmission rod lines were incorporated into growing sea ice. This arrangement would also eliminate any effect that an air gap may have produced in the earlier sea ice test results. Early in November 1980, three "ladder" arrays (Figs. 14 and 15) were suspended from the thin sea ice surface. Two ladders were installed at a site just north of Prudhoe Bay at the old site of the manmade Exxon experimental sea ice island (Reimnitz et al. 1982). One ladder was oriented north-south and the other east-west. The third ladder was installed in Prudhoe Bay about 100 m west of the East Dock. Each two-conductor transmission line was fed and terminated by an equal length of 50-ohm coaxial cable. This allowed both transmission and reflection measurements to be made. Figure 16 shows the 50-ohm cables on the surface and the top set of two-conductor transmission lines on one of the ladders.

Examples of the TDR and TDT data are shown in Figures 17 and 18 respectively. As would be expected, the amplitude and rise front of the voltage step pulse decreases with depth in the sea ice due to an increase in brine volume and a related increase in the conductivity of the sea ice. A plot of the low-frequency coefficient of reflection data vs depth for the two sites is shown in Figure 19. Here too the exponential increase in the coefficient of reflection with depth is due to brine volume and conductivity effects. Related salinity, temperature, and brine volume profiles are given in Figure 20.

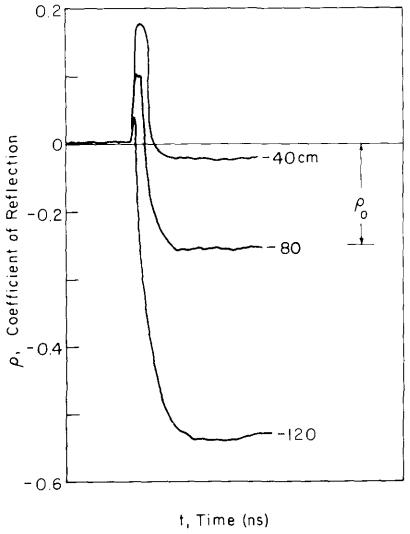

Figure 17. Examples of the coefficient of reflection as a function of time at three depths in sea ice at the East Dock site. ρ_o is the low-frequency value of ρ.

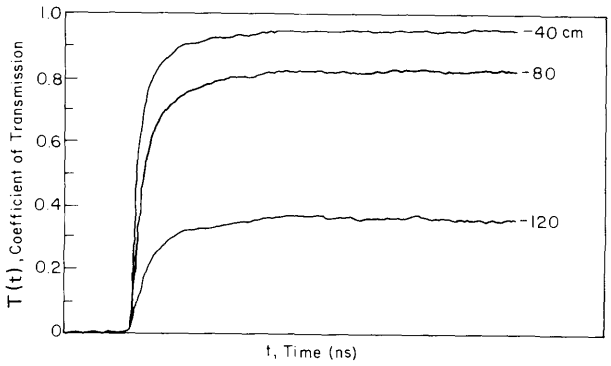

Figure 18. Examples of the coefficient of transmission as a function of time at three depths in sea ice at the East Dock site.

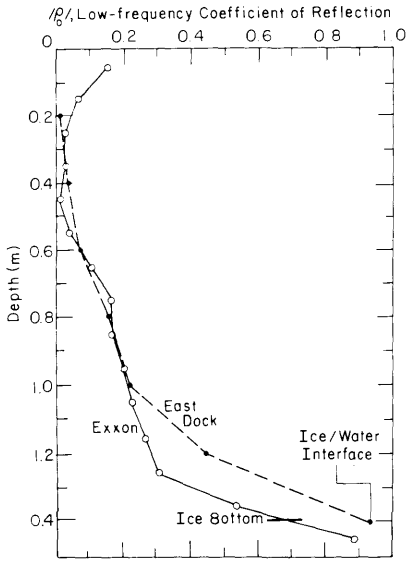

Figure 19. Magnitude of the low-frequency coefficient of reflection as a function of depth for the ladder arrays at the Exxon and East Dock sites.

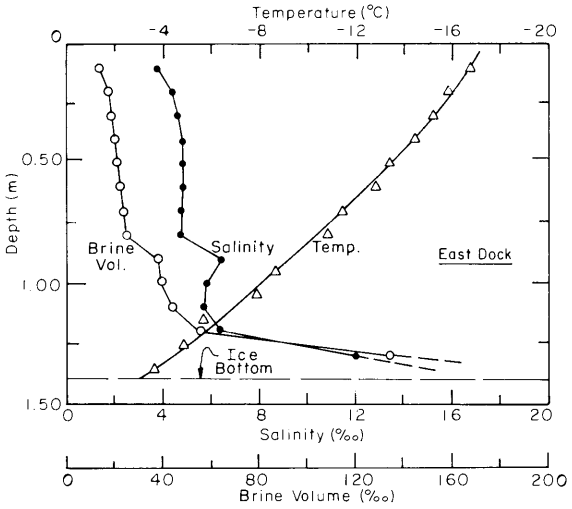

a. East Dock site.

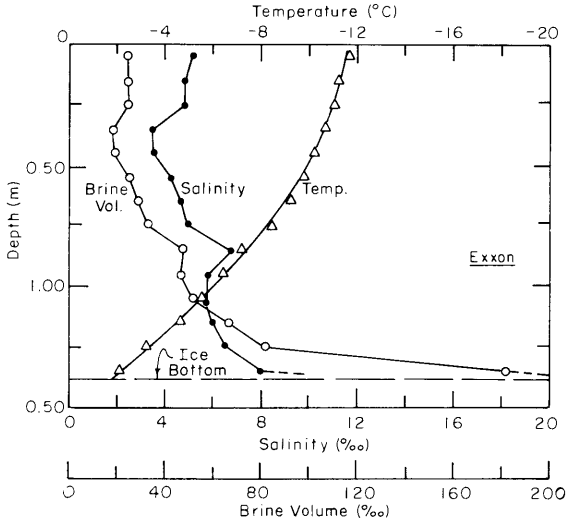

b. Exxon site.

Figure 20. Temperature, salinity, and brine volume as a function of depth.

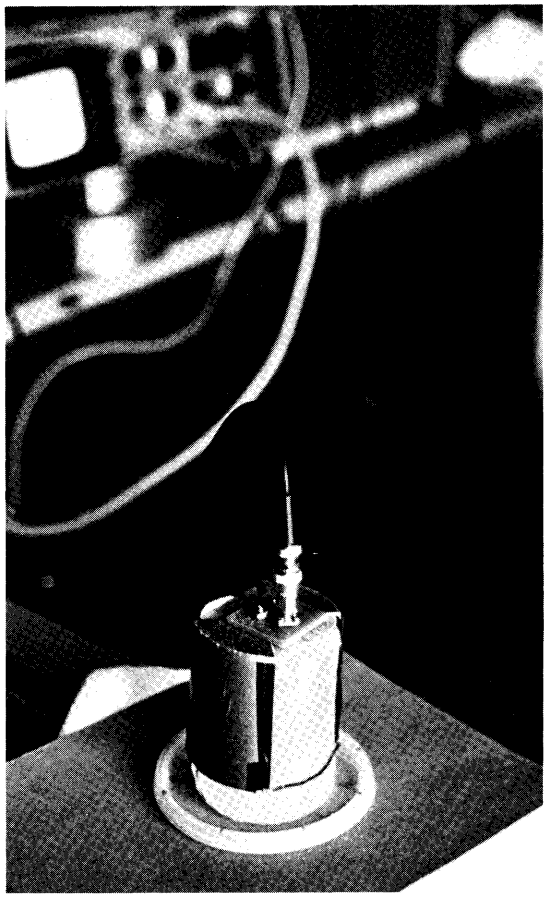

Figure 21. Photograph showing the quadrant arc transmission line cell with a sea ice core sample in the cell.

An ice core from each site was evaluated using the quadrant arc transmission line configuration (Fig. 5d). Core sections 10 cm long were inserted into the cell (Fig. 21), and TDR measurements were made every 20° of arc around the core. The relative voltage amplitude of the reflection from the open end of the cell was recorded and plotted as shown in Figure 22. When the electric field in the cell was parallel to the preferred *c*-axis direction or perpendicular to the general alignment of the brine pockets in the sea ice crystals, a maximum reflection occurred from the bottom of the cell. The relative amplitude of this reflection is an indication of the degree of anisotropy in the ice. Table 1 indicates that the degree of anisotropy is greatest at or near the bottom of the sea ice.

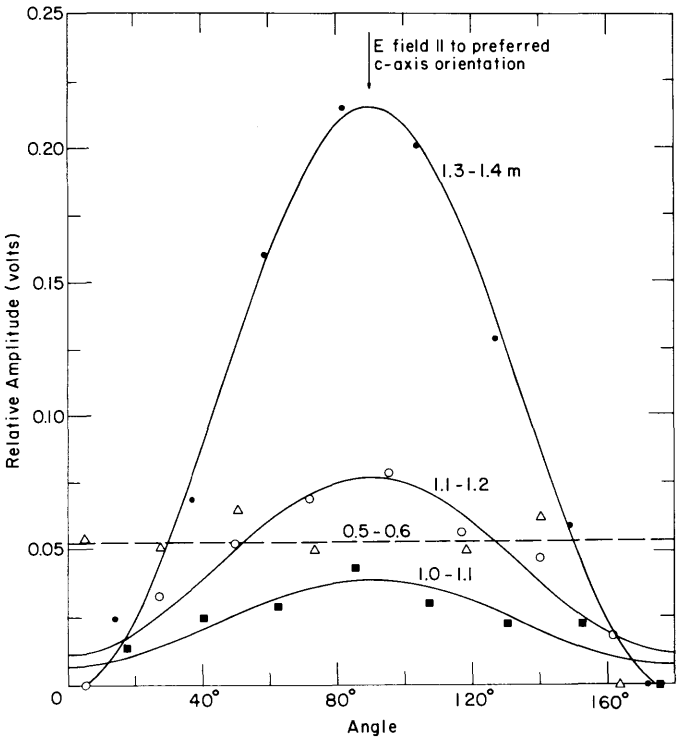

a. East Dock site.

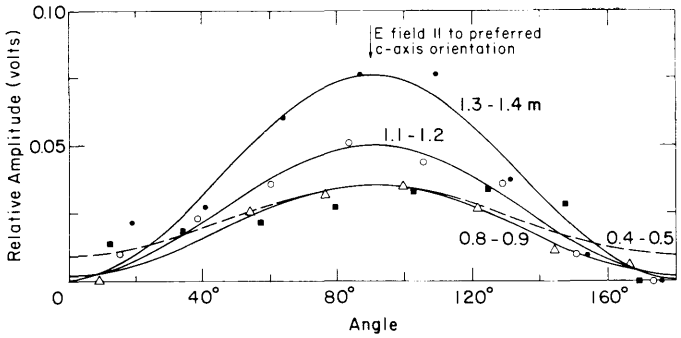

b. Exxon site.

Figure 22. Relative amplitude as a function of angle and depth for TDR cell measurements of sea ice core.

Table 1. Summary of time-domain reflection cell data analysis.

Sample depth (m)	*Rel. peak amplitude (V)*	*C-axis orientation observations*
Exxon site		
0.20–0.30	0.61	Bubbly ice on top, random *c*-axis on bottom
0.40–0.50	0.26	
0.60–0.70	0.14	Weak crystal *c*-axis orientation
0.80–0.90	0.34	Crystals *c*-axis oriented
1.00–1.10	0.13	Weak crystal *c*-axis orientation
1.10–1.20	0.48	Strong crystal *c*-axis orientation
1.20–1.30	0.85	Strong crystal *c*-axis orientation
1.30–1.40	0.76	Strong crystal *c*-axis orientation
East Dock site		
1.00–1.10	0.32	
1.10–1.20	0.66	
1.30–1.40	2.17	

ANALYSIS OF LADDER DATA

The transmission line measurements from the two 1980 ladder sites were analyzed using the following equation for the frequency-domain coefficient of transmission $T(j\omega)$:

$$T(j\omega) = \tau_{12}(j\omega)\,\tau_{21}(j\omega)\exp(-\gamma_2 \ell) \tag{19}$$

where $\tau_{12}(j\omega)$ = transmission coefficient at junction of 50-ohm coaxial cable and two-wire line
$\gamma_2 = \alpha + j\beta$ = propagation constant through ice encompassing the two-wire line
ℓ = length of the two-wire line (20 cm)
$\tau_{21}(j\omega)$ = transmission coefficient at junction of two-wire line and the 50-ohm coaxial cable.

The characteristic impedance Z_c of the two-wire line is:

$$Z_c = (\eta_2/\pi)\cosh^{-1}(b/a) \tag{20}$$

where η_2 = intrinsic complex impedance of the two-wire line $(= j\omega\mu_2'/\gamma_2)$
b = line separation
a = diameter of conductor.

The transmission coefficients are

$$\tau_{12}(j\omega) = \frac{2Z_o}{Z_o+Z_c} = 1-\rho(j\omega) \tag{21}$$

and

$$\tau_{21}(j\omega) = \frac{2Z_c}{Z_o+Z_c} \tag{22}$$

where Z_o = 50 ohms.

Using eqs 20, 21, and 22, eq 19 can be written as

$$T(j\omega) = \frac{4Z_o(\eta_2/\pi)\cosh^{-1}(b/a)}{[Z_o+(\eta_2/\pi)\cosh^{-1}(b/a)]^2}\exp(-\gamma_2\ell)\,. \tag{23}$$

Likewise, the coefficient of reflection is

$$\rho(j\omega) = \frac{\eta_2\cosh^{-1}(b/a)-Z_o\pi}{\eta_2\cosh^{-1}(b/a)+Z_o\pi}\,. \tag{24}$$

At low frequencies ($<\sim$20 MHz), η_2 and γ_2 are essentially independent of the dielectric constant of the sea ice. Therefore, the low-frequency conductivity (or DC conductivity) of the sea ice can be calculated using eq 23 and the measured transmission data. At higher frequencies (100 to 300 MHz), the coefficient of transmission is dependent on the dielectric constant, conductivity, and frequency. For this frequency range, the time-domain transmission results were converted to the frequency domain using a spectrum analyzer. The slope of the resulting relative attenuation A_r vs frequency curve (Fig. 23 and Table 2) was then used in eq 23 to estimate the real part of the dielectric constant.

Table 2. Slope of relative attenuation curve from 100 to 300 MHz vs probe depth and the associated correlation coefficient.

Probe depth (m)	*100-300 MHz slope (dB/MHz)*	*Corr. coeff. (r)*
Exxon site		
0.05	0.00607	0.9011
0.15	0.00195	0.4102
0.25	0.00227	0.5421
0.35	0.00063	0.1226
0.45	0.00177	0.4279
0.55	0.00188	0.4685
0.65	0.00379	0.7389
0.85	0.00594	0.7587
0.95	0.00667	0.8685
1.05	0.00407	0.6762
1.15	0.00622	0.8638
1.25	0.00622	0.8222
1.35	0.0128	0.9793
1.45	0.0101	0.2846
East Dock site		
0.20	0.00019	0.0592
0.40	0.00236	0.5432
0.60	0.00321	0.7474
0.80	0.00473	0.6247
1.00	0.00454	0.8179
1.20	0.00626	0.8387
1.40	0.0154	0.4921
1.60	0.0179	0.1895

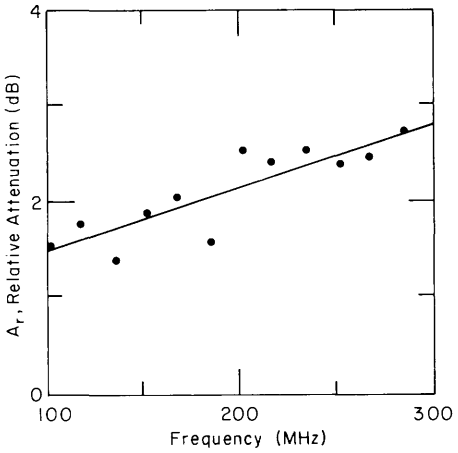

Figure 23. Example of relative attenuation as a function of frequency derived from time-domain transmission data.

Conductivity of brine and sea ice

The dissolved solids in sea water consist primarily of six salts, of which NaCl makes up about 68% (Assur 1960). Since little information is available on the ionic conductivity of brine at low temperatures ($< -5°C$), expressions for the conductivity of concentrated NaCl solutions are used (Stogryn 1971). These are

$$\sigma_{NaCl}(T,N) = \sigma_{NaCl}(25,N)\,[1.000 - 1.962\times10^{-2}\Delta + 8.08\times10^{-5}\Delta^2 - \Delta N\{3.020\times10^{-5} + 3.922\times10^{-5}\Delta + N(1.721\times10^{-5} - 6.584\times10^{-6}\Delta)\}] \quad (25)$$

where $\Delta = 25 - T$ (T = temperature, °C) and

$$\sigma_{NaCl}(25,N) = N\,[10.394 - 2.3776N + 0.68258N^2 - 0.13538N^3 + 1.0086\times10^{-2}N^4]$$

and normality N is

$$N = S_b\,[1.707\times10^{-2} + 1.205\times10^{-5}S_b + 4.058\times10^{-9}S_b^2]$$

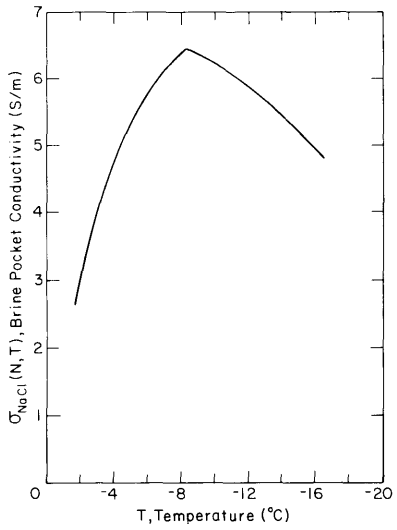

Figure 24. Brine pocket conductivity as a function of temperature.

where S_b is the brine salinity in parts per thousand and is valid for $0 < S_b \leq 260$ (Stogryn 1971). The salinity of the brine in sea ice S_b was derived from data given by Assur (1960):

$$S_b = 9.65 - 14.8T; \quad -8.2 \leq T \leq -20°C \qquad (26)$$

$$S_b = 78.11 - 6.60T; \quad -22.9 \leq T \leq -8.2°C \qquad (27)$$

A plot of the NaCl brine conductivity in ice vs temperature, as calculated from eqs 25, 26, and 27, is shown in Figure 24. As expected, the solution conductivity begins to increase with decreasing temperature since the brine salinity has to increase to maintain phase equilibrium. However, below about –8°C, conductivity decreases with decreasing temperature, even though the salinity is still increasing. The increase in conductivity to be expected due to the increase in salinity is more than compensated for by the decrease in conductivity due to the decrease in temperature. The conductivity of a NaCl solution increases about 0.02/°C, so that the ionic conductivity for a temperature other than 25°C is given by

$$\sigma_{NaCl}(T) = \sigma(25°C)\,[1 + \beta(T - 25°)]$$

where $\beta \approx 2 \times 10^{-2}$ per °C. This brine conductivity will be used in calculating the complex dielectric constant of the liquid in sea-ice brine pockets.

Sea ice conductivities were determined using the TDT measurements and eqs 1 and 23. The results are listed in Table 3. The conductivity of the sea ice as a function of brine volume is plotted in Figure 25. To find the best fit to all the data, several correlation functions, including power

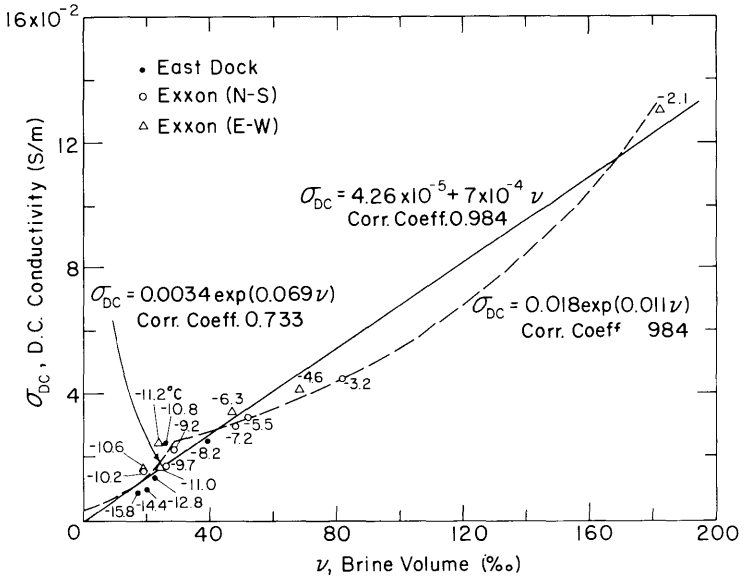

Figure 25. DC conductivity as a function of brine volume. Solid line is the linear least-squares fit. Dashed lines are exponential fits to the data above and below about the 80-cm depth.

Table 3. Brine volume, DC conductivity, and relative real dielectric constant at various ladder probe depths in the sea ice (ϵ'_{rm} using eq 23).

Probe depth (m)	*Brine volume v (‰)*	*Conductivity σ_{DC} (S/m)*		*Dielectric constant ϵ'_{rm}*
		TDT data	*TDR data*	
Exxon site, 1980				
North-south rods				
0.25	25	1.66×10^{-2}		3.6
0.45	19	1.55×10^{-2}		3.8
0.65	29	2.2×10^{-2}		3.45
0.85	48	2.9×10^{-2}		3.3
1.05	52	3.2×10^{-2}		5.2
1.25	82	4.45×10^{-2}		4.7
1.45	Sea water	4.0×10^{-1}	2.8	40
East-west rods				
0.15	24	2.4×10^{-2}		4.5
0.35	19	1.66×10^{-2}		4.0
0.55	25	1.66×10^{-2}		3.9
0.75	33	–		–
0.95	47	3.35×10^{-2}		3.4
1.15	68	4.1×10^{-2}		4.35
1.35	182	1.3×10^{-1}		8.4
East Dock site, 1980				
0.20	17	9×10^{-3}		5.5
0.40	20	1×10^{-2}		2.4
0.60	22	1.3×10^{-2}		2.63
0.80	25	2.4×10^{-2}		3.50
1.00	39	2.5×10^{-2}		3.72
1.20	56	6.8×10^{-2}		7.6
1.40	Ice/water interface	2.75	5.53	88.9
1.60	Sea water	3.0	5.19	88.9

and exponential, were tried. The linear equation was found to give the best fit. At zero brine volume, the conductivity is 4.26×10^{-5} S/m, which is within the range for "pure" ice. The data in Figure 25 indicate a rapid increase in DC conductivity to a brine volume of 30‰ followed by a gradually increasing trend. The break in the data occurs at a depth of ≈80 cm or a temperature of about –8°C. Exponential correlations were found to fit the σ_{DC} data, below and above a brine volume of 30‰, with the highest correlation coefficient. The equations so obtained and their respective curves are also shown in Figure 25.

At about –8.2°C a phase change occurs in the brine where mirabilite ($Na_2SO_4\cdot10\,H_2O$) begins to precipitate out of solution (Assur 1960). This dissolved salt is a contributor to the measured conductivity, and when it begins to precipitate it seems to affect the rate of change in the DC conductivity as noted. "Pure" ice has a DC conductivity of about 2.6×10^{-8} S/m at -19°C (King and Smith 1981). Measurements on polar ice indicate values ranging from 10^{-5} to 10^{-4} S/m (Walford 1968, Bentley 1977). The residual DC conductivity of 3.4×10^{-3} S/m at zero brine volume from our data is due in part to the limited data from which to construct what may be a more representative curve. However, the higher DC conductivity of the zero brine volume, which was obtained from the curve passing through our brine volume data below 30‰, may be due to an interfacial phenomenon taking place at the interface of ice and brine, as suggested by Sen et al. (1981) to explain a similar residual effect they observed in their study of glass beads placed in saline water. If σ_{DC} were only a function of the brine volume, this explanation would be appropriate. However, σ_{DC} also depends on the shape and distribution of the brine inclusions, which are not controlled. The scatter is most likely due to this effect, and σ_{DC} ($v = 0$) as determined by the least-squares fit is only approximate.

Several empirical equations have been produced to describe the relationship of the formation factor to porosity in brine-saturated soil and rock (Archie 1942). This same analysis is now applied to sea ice. The DC conductivity of sea ice can be stated in terms of a formation factor (FF):

$$FF = \frac{\text{conductivity of the brine}}{\text{conductivity of the sea ice}} = \frac{\sigma_b}{\sigma_{si}}. \tag{28}$$

Archie (1942) found an empirical expression for porous rock

$$FF = \phi^{-m} \tag{29}$$

where ϕ is the porosity or fractional volume of water, and m is a constant. Jackson et al. (1978) found that the exponent m was dependent on the shape of the host particles (sand), increasing as the particles become less spherical. Sen et al. (1981) show that $m = 1.5$ for spherical particles, is greater than 1.5 for plate-like grains or cylinders whose major axis is perpendicular to an electric field, and is less than 1.5 when the electric field is parallel to the major axis of the plate-like grains.

Since we have an estimate of the conductivity of the brine (eqs 25, 26, and 27, Fig. 24) and have measured the liquid-filled void porosity (brine volume) and conductivity of the sea ice (Fig. 25), m can be calculated from eqs 28 and 29. Figure 26 is a plot of the sea ice formation factor as a function of porosity. The best least-squares fit to the data indicates that $m = 1.55$ in the top 80 cm of the sea ice and $m = 1.75$ in the lower section of the sea ice. The exponent m tended to increase with increasing depth in the sea ice, as indicated by the data in Figure 26. Archie's rule implies that this increase in m indicates that the sea ice structure changed from a spherical or elliptical geometry to a vertical platey or cylindrical geometry. As related to known sea ice structure,

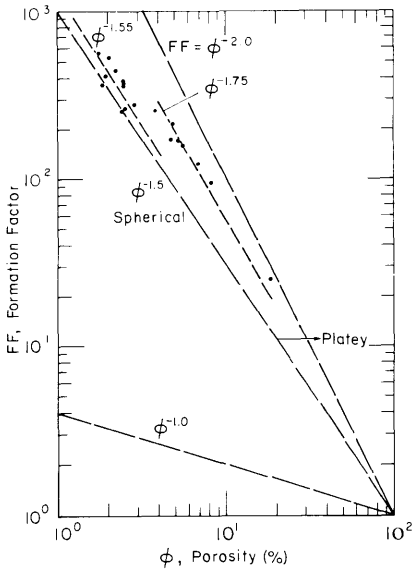

Figure 26. Formation factor as a function of porosity.

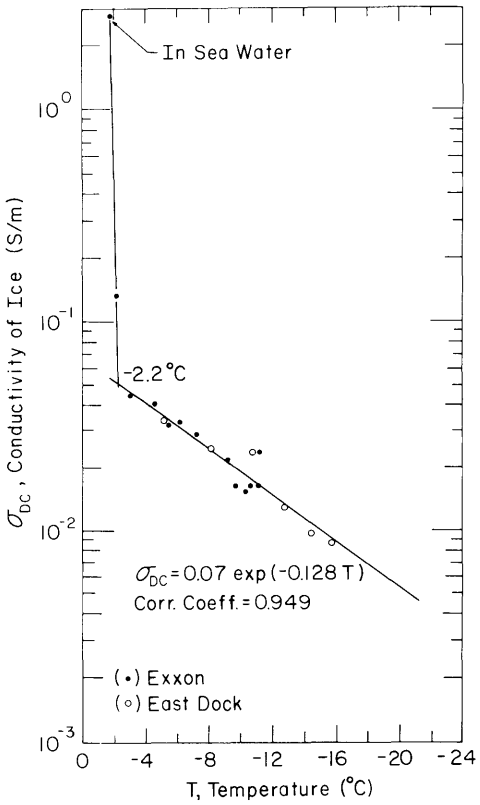

Figure 27. Measured DC conductivity of sea ice as a function of temperature.

the results can be interpreted to indicate that the *c*-axis of the ice crystals, and therefore the minor axis of the ice platelets, rotated from a predominantly vertical orientation near the top of the ice sheet to a more horizontal orientation with increasing depth (Weeks and Gow 1978).

By combining eqs 28 and 29, Archie's rule provides a means for estimating the DC conductivity of sea ice from the brine volume. Likewise, the bulk brine volume could be estimated using the sea ice conductivity measurements.

The measured sea ice conductivity as a function of temperature is shown in Figure 27. Note the abrupt change in the slope through the data at -2.2°C. This is of interest since it appears to be the depth at which radar reflections from the bottom of sea ice occur (Kovacs and Morey 1978, 1979). From a radar profiling standpoint, the reflections are not coming from the sea ice/water interface but from a zone several centimeters up in the ice at a specific temperature and conductivity.

Complex dielectric constant of brine and sea ice

The relative complex dielectric constant of the brine was calculated using eq 7. Expressions given by Stogryn (1971) for NaCl solutions were used to approximate the relative static dielectric constant ϵ_{rsb} and the relaxation time τ_b of the brine as follows:

$$\epsilon_{rsb}(T,N) = \epsilon_{rsb}(T,0)\,[1.000 - 0.2551N + 5.151\times10^{-2}N^2 - 6.889\times10^{-3}N^3] \tag{30}$$

and

$$\tau_b(T,N) = \tau_b(T,0)\,[0.1463\times10^{-2}NT + 1.000 - 0.04896N - 0.02967N^2 + 5.644\times10^{-3}N^3] \tag{31}$$

where, from the data presented by King and Smith (1981), $\epsilon_{rsb}(T,0)$ and $\tau_b(T,0)$ were calculated to be respectively:

$$\epsilon_{rsb}(T,0) = 88.22 - 0.4105T + 0.0008T^2 + 1.0879\times10^{-6}T^3$$

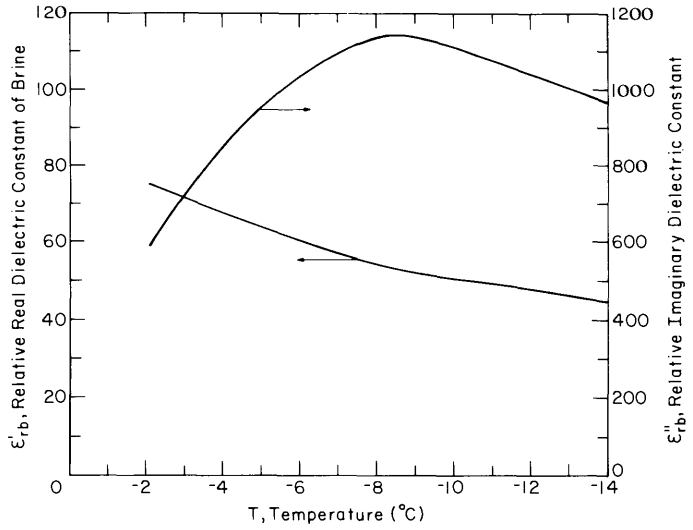

Figure 28. Calculated relative real and imaginary dielectric constants of brine at 100 MHz.

and

$$\tau_b(T, 0) = 17.80\times10^{-12} - 0.6032\times10^{-12}\,T + 0.0109\times10^{-12}\,T^2 - 0.0001\times10^{-12}\,T^3$$

in the temperature range $-10^\circ \leqslant T \leqslant 20^\circ$C.

Figure 28 is a plot of the real and imaginary parts of the relative complex dielectric constant of brine ϵ^*_{rb} at 100 MHz as a function of temperature. Note that ϵ''_{rb} becomes depressed with decreasing temperature and has relatively large values. As an example, at -10°C and a frequency of 100 MHz, $\epsilon^*_{rb} = 50 - j1110$, whereas the relative complex dielectric constant for typical sea water ϵ^*_{rw} at 0°C and 100 MHz is $\epsilon^*_{rw} = 76 - j551$. The decrease of ϵ^*_{rb} with decreasing temperature, as determined from eq 7, is due to the decrease in the value of ϵ_{rsb} with decreasing temperature as determined from eq 30 and used in eq 7. The real part of the dielectric constant of sea ice as determined from the TDS measurements will be discussed next and then a mixing model will be presented from which the imaginary part of the dielectric constant of sea ice can be estimated.

The TDT data were used to calculate the slope of the relative attenuation vs frequency data (Table 2), as explained earlier. The real part of the relative dielectric constant for the sea ice mixture ϵ'_{rm} was then calculated using eq 23; and the data that gave a correlation coefficient of over 0.3 in Table 2. Equation 23 contains the intrinsic complex impedance of a dielectrically loaded transmission line, which in turn is a function of the complex propagation constant γ, eq 1. The results are listed in Table 3 and plotted in Figure 29. Even though there is scatter to the data, a weak trend appears to exist between the N-S and E-W values that may be explained by the anisotropy of the sea ice.

Radar anisotropy measurements (Kovacs and Morey 1979, 1980) were made at the Exxon site at the same time that the TDS measurements were made. The maximum voltage amplitude of the reflected radar signal was 122° vs 128° ±10° for the preferred *c*-axis direction of the sea ice crystal platelets at the bottom of the sea ice (see Fig. 30). It has been demonstrated that maximum radar return occurs when the electric field is parallel to the preferred *c*-axis direction (Kovacs and Morey 1978, 1979, 1980). When the rods were N-S the electric field was E-W, primarily parallel to the preferred crystal *c*-axes. When the electric field was N-S (rods E-W), it was primarily parallel to the vertical, plate-like structure formed by the brine inclusions. The dielectric constant should be lower when the electric field is parallel to the *c*-axis (rods N-S) and perpendicular to the plate-like structure formed by the brine inclusions, as is shown in Figure 29, implied in Figure 4, and modeled in Figure 8. The slope of the ϵ'_{rm} vs v line passing through the N-S data in Figure 29 should also

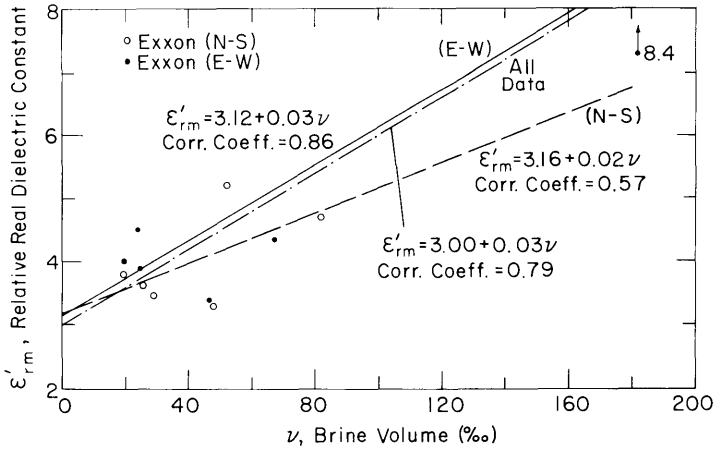

Figure 29. Relative real dielectric constant of sea ice-brine mixture vs brine volume as a function of two-conductor transmission line orientation. Solid lines are the linear least-squares fits to the Exxon N-S and E-W data.

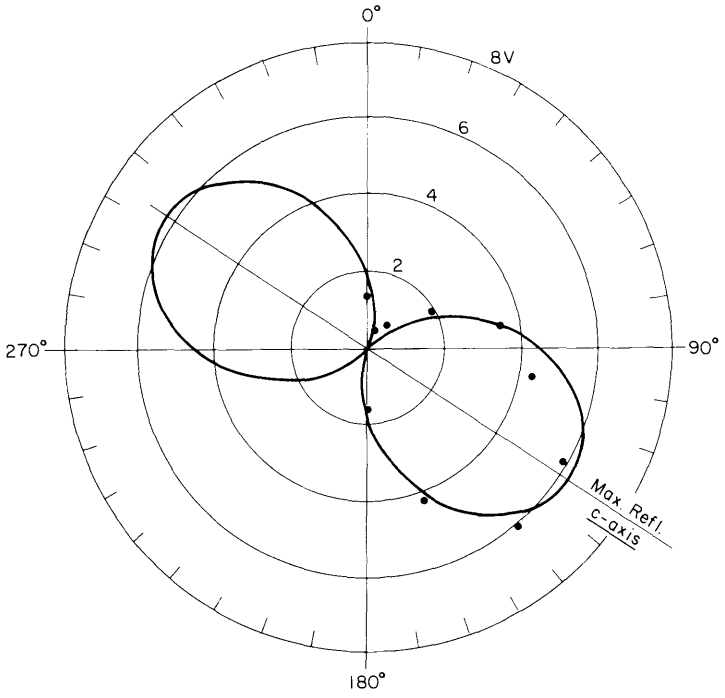

Figure 30. Voltage amplitude of the radar EM wavelet reflected from the ice antenna E-field azimuth at the Exxon site. The "lemniscate" curve fits the data with a correlation coefficient of 0.975. The major axis is at 122°.

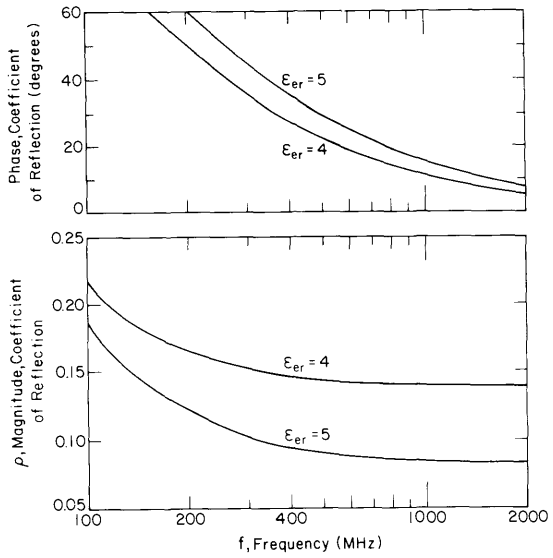

Figure 31. Magnitude and phase of the coefficient of reflection as a function of frequency for $\epsilon_{er} = 4$ and 5 and $\sigma_e = 2.5 \times 10^{-2}$ S/m.

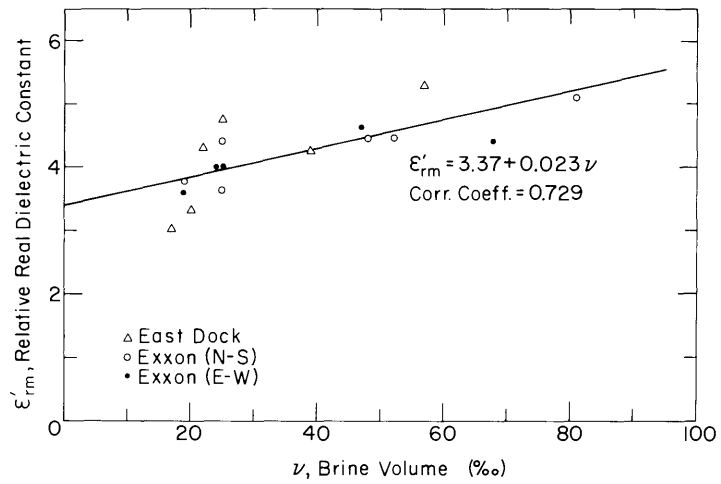

Figure 32. The relative real dielectric constant of sea ice-brine mixture as a function of brine volume. The solid line is a linear least-squares fit to all the data.

Table 4. Brine volume, DC conductivity, and the relative dielectric constant as a function of ladder probe depth in the sea ice (ϵ'_{rm} using eq 24).

Probe depth (m)	*Brine volume v (‰)*	*Conductivity σ_{DC} (S/m)*		*Dielectric constant*
		TDT data	*TDR data*	ϵ'_{rm}
Exxon site, 1980				
North-south rods				
0.25	25	1.66×10^{-2}		3.6
0.45	19	1.55×10^{-2}		3.75
0.65	29	2.2×10^{-2}		4.4
0.85	48	2.9×10^{-2}		4.45
1.05	52	3.2×10^{-2}		4.45
1.25	82	4.45×10^{-2}		5.1
1.45	Sea water	4.0×10^{-1}		(88.9)
East-west rods				
0.15	24	2.4×10^{-2}		4.0
0.35	19	1.66×10^{-2}		3.6
0.55	25	1.66×10^{-2}		4.0
0.75	33	–		–
0.95	47	3.35×10^{-2}		4.6
1.15	68	4.1×10^{-2}		4.4
1.35	182	1.3×10^{-1}		
East Dock site, 1980				
0.20	17	9×10^{-3}		3.0
0.40	20	1×10^{-2}		3.3
0.60	22	1.3×10^{-2}		4.3
0.80	25	2.4×10^{-2}		4.75
1.00	39	2.5×10^{-2}		4.25
1.20	56	6.8×10^{-2}		5.3
1.40	Ice/water interface	2.75	5.53	–
1.60	Sea water	3.0	5.19	–

be less than the slope of the line passing through the E-W data, as is the case. These effects are most evident at the higher brine volumes that occur deeper in the ice where the anisotropy is greater.

The real part of the dielectric constant was also estimated from the TDR data. As the examples in Figure 17 show, the initial reflections are positive but decrease in amplitude and become narrower with sounding depth as the sea ice increases in conductivity and dielectric constant. This implies that the low frequencies have a 180° phase shift, while the highest frequencies do not. For a lossless material ($\sigma_e = 0$), the magnitude of the coefficient of reflection is independent of frequency, being only dependent on ϵ_{er}, and the phase angle of the coefficient of reflection is 0°. Values of $\rho(j\omega)$, calculated from eq 24, are plotted in Figure 31 as a function of frequency for two values of ϵ_{er} and one value of σ_e. At high frequencies (750-2000 MHz), ϵ_{er} primarily determines the magnitude of ρ for the range of conductivities measured in the sea ice. Therefore, the amplitude of the initial positive pulse in the TDR data was used to calculate (eq 24) the real part of the dielectric constant. The results are listed in Table 4. A plot of ϵ'_{rm} as a function of brine volume is given in Figure 32. There is less scatter to the

data than in Figure 29, and the higher values obtained for ϵ'_{rm} seem to be more reasonable than some of the values listed in Table 3 as determined from the TDT measurements.

The relative complex dielectric constant for a two-component system (ice and brine) is proportional to the relative dielectric constants of each of the components weighted by their relative volumes. There are several dielectric mixing formulas, but the one that seems most appropriate for sea ice was proposed by Tinga et al. (1973) and used by Vant et al. (1978) and Golden and Ackley (1980):

$$\epsilon^*_{rm} = \epsilon'_{rm} - j\epsilon''_{rm} = \epsilon^*_{ri} + \left[\frac{v\epsilon^*_{ri}(\epsilon^*_{rb} - \epsilon^*_{ri})}{n(1-v)(\epsilon^*_{rb} - \epsilon^*_{ri}) + \epsilon^*_{ri}}\right] \tag{32}$$

where ϵ^*_{rm} = relative complex dielectric constant of the mixture (sea ice)
ϵ^*_{ri} = relative complex dielectric constant of pure ice (≈ 3.14)
ϵ^*_{rb} = relative complex dielectric constant of brine
v = brine volume
n = depolarization factor.

The dielectric constant of brine has been shown to change with temperature (Fig. 28) and therefore it changes in winter sea ice, since temperature increases with depth.

The depolarization factor is not known, but can be estimated from our measurements. Using the ϵ'_{rm} data in Table 4, eq 7 for ϵ^*_{rb}, and first assuming $\epsilon''_{rm} = 0$, the depolarization factor was calculated from

$$n = \frac{\epsilon^*_{ri}}{(1-v)} \frac{v}{(\epsilon^*_{rm} - \epsilon^*_{ri})} - \frac{1}{(\epsilon^*_{rb} - \epsilon^*_{ri})} \tag{33}$$

Then eq 32 was used to recalculate ϵ^*_{rm}. This iterative process resulted in the calculated ϵ'_{rm} and ϵ''_{rm} values that are listed in Table 5 along with the depolarization factor.

The depolarization factor is a measure of both the shape and the orientation of the brine inclusions with respect to the external electric field. For three idealized cases, the depolarization factor is 0 for needles, $^1/_3$ for spheres, and 1 for plates (Sen et al. 1981). If one assumes that in the vertical plane the brine pockets are ellipsoidal in nature (e.g. Vant et al. 1978), then the plot of n as a function of depth (Fig. 33) implies that on average the major axis of the ellipsoids is tilted at some angle from the vertical. For example, if the brine pockets were vertical cylinders or vertical ellipsoids, then n would tend toward $^1/_3$. (Note that the electric field between the rods was horizontal.) The depolarization factor clusters around 0.1, implying that on average the major axis of the ellipsoids is tilted more than 45° from the vertical. In their analysis of transmission line data obtained from measurements on sea ice samples, Vant et al. (1978)

Table 5. Depolarization factor (n), real (ϵ'_r), and imaginary (ϵ''_r) dielectric constant calculated at 100 MHz vs ladder probe depth in sea ice and measured ϵ'_{rm}.

Probe depth (m)	*Measured* ϵ'_{rm}		*Calculated*	
		n	ϵ'_{rm}	ϵ''_{rm}
Exxon site, 1980				
0.15	4.0	0.091	4.0	28.1×10^{-3}
0.25	3.6	0.148	3.7	10.8×10^{-3}
0.35	3.6	0.129	3.6	10.4×10^{-3}
0.45	3.75	0.101	3.75	17.4×10^{-3}
0.55	4.0	0.092	4.0	26.9×10^{-3}
0.65	4.4	0.0736	4.4	48.6×10^{-3}
0.85	4.45	0.122	4.45	31.9×10^{-3}
0.95	4.6	0.106	4.6	42.7×10^{-3}
1.05	4.45	0.131	4.45	33.0×10^{-3}
1.15	4.4	0.182	4.4	25.3×10^{-3}
1.25	5.1	0.142	5.1	61.8×10^{-3}
East Dock site, 1980				
0.20	3.0	0.397	3.28	1.27×10^{-3}
0.40	3.3	0.406	3.3	1.33×10^{-3}
0.60	4.3	0.061	4.3	59.7×10^{-3}
0.80	4.75	0.051	4.74	92.2×10^{-3}
1.00	4.25	0.114	4.25	27.6×10^{-3}
1.20	5.3	0.086	5.3	85.4×10^{-3}

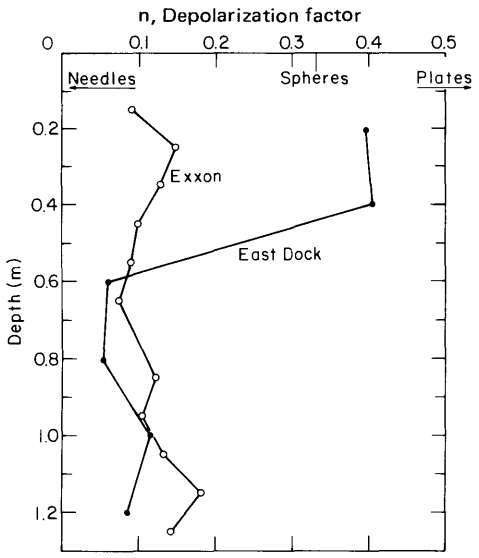

Figure 33. The depolarization factor as a function of depth at the Exxon and East Dock sites.

concluded that the brine ellipsoids were "oriented at an angle of between 35° and 45° to the vertical." There is no reported physical evidence indicating that the brine pockets in sea ice are so inclined. However, as stated earlier, the brine drainage channels in sea ice are inclined at an average slope of 45°. These healed and active channels, by themselves or in association with the spatial arrangement of the individual brine pockets that they drain, may be contributing to the depolarization factor of about 0.1 as noted.

The calculated relative real dielectric constant from Table 5 is plotted in Figure 34 as a function of brine volume. Also shown are the two cases of parallel and perpendicular orientation of nonconductive needles from eqs 9 and 10 as illustrated in Figure 4. Note that the least-squares fit line through the data tends toward the vertical orientation, implying that the major axes of the polarizing elements in the sea ice are inclined less than 45° from the vertical. Figure 35 is a plot of ϵ'_{rm} as a function of n. The lower correlation coefficient, while not significant statistically, suggests that the relative real dielectric constant is not as dependent upon the orientation of the brine pockets as it is on the brine volume.

Figure 36 shows graphically the relationship between the ϵ''_{rm} and n values listed in Table 5, indicating the relatively strong correlation between the loss factor in sea ice and the orientation and shape of the brine inclusions. Poor correlation was found between ϵ''_{rm} and brine volume. These results support the radar sounding measurements of Kovacs and Morey (1980) wherein the attenuation of the radar signal in anisotropic sea ice was dependent upon the orientation of the electric field to the preferred horizontal *c*-axis orientation of the sea ice crystals. There was no detectable time-of-flight anisotropy, which would have occurred if the real part of the dielectric constant were strongly influenced by the preferred orientation of the sea ice crystals and brine pockets

The calculated ϵ'_{rm} and ϵ''_{rm} information at 100 MHz in Table 5 and the measured σ_{DC} values in Table 4 were used in eqs 1, 2, and 3 to calculate the velocity of propagation and attenuation

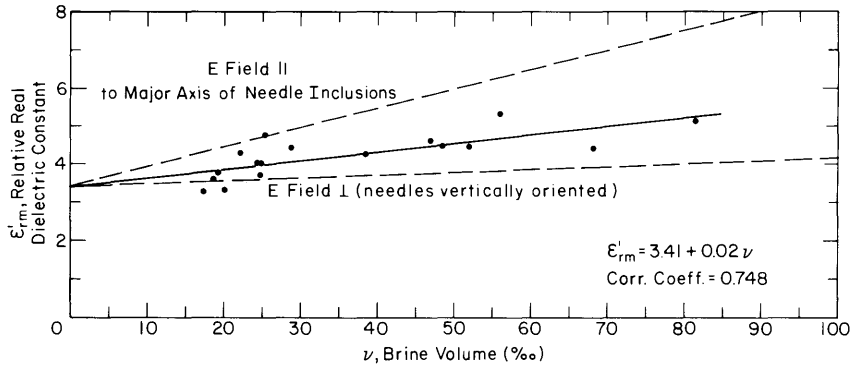

Figure 34. The calculated relative real dielectric constant of the sea ice-brine mixture as a function of brine volume. The calculation was made at 100 MHz using the depolarization factor (eq 32).

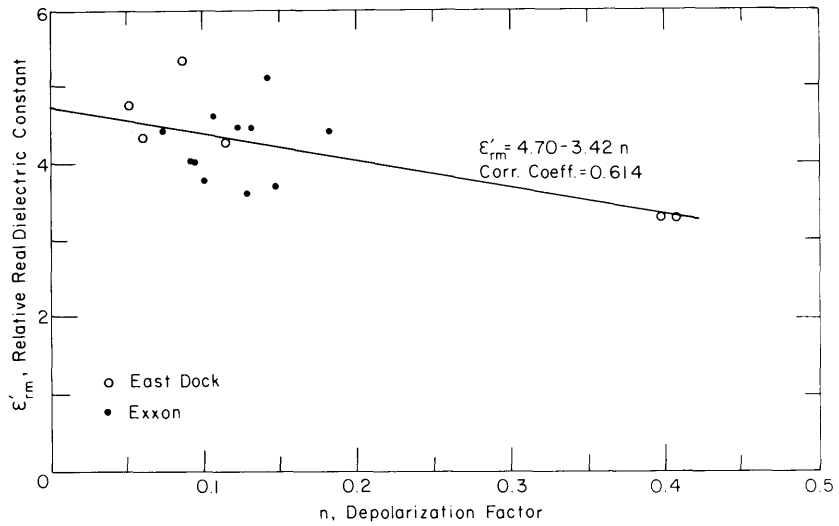

Figure 35. The calculated relative real dielectric constant of the sea ice-brine mixture as a function of the depolarization factor.

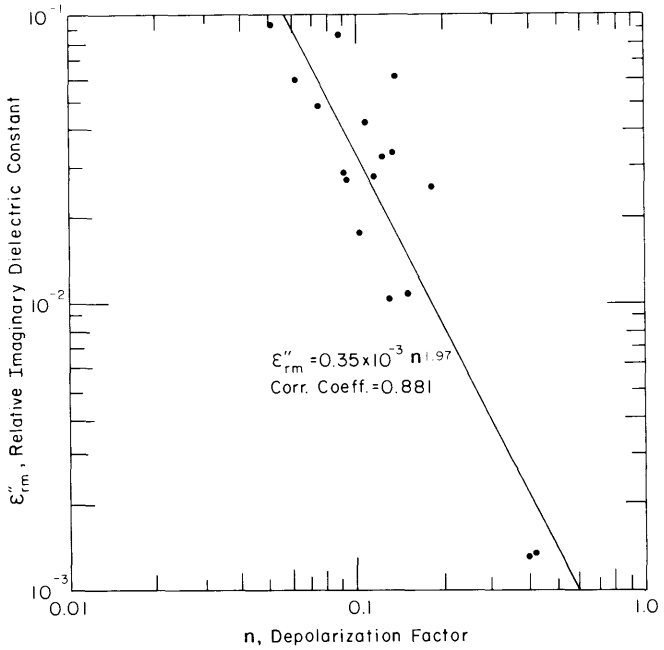

Figure 36. The calculated relative imaginary dielectric constant of the sea ice-brine mixture as a function of the depolarization factor.

rate of the EM signal in the sea ice. The data in Table 6 show that signal attenuation increases and velocity decreases, as would be expected with depth or increasing brine volume. Attenuation as a function of brine volume is shown in Figure 37. Since attenuation is primarily determined by conductivity, the shape of the curve should be similar to Figure 25, and for the same reasons discussed previously. As can be seen, the losses increase rapidly with increasing brine volume to $\approx 30^{0}/_{00}$, or in the top 80 cm ($T < -8^{\circ}$C), and less rapidly above a brine volume of $\approx 30^{0}/_{00}$, or in the bottom 80 cm ($T > -8^{\circ}$C).

Table 6. Attenuation rate and effective velocity of propagation calculated at 100 MHz as a function of ladder probe depth in sea ice.

Probe depth (m)	*Brine volume v (‰)*	*Attenuation A (dB/m)*	*Velocity v_e (m/ns)*
Exxon site, 1980			
0.15	24	17.67	0.135
0.25	25	13.36	0.147
0.35	19	13.36	0.147
0.45	19	12.36	0.146
0.55	25	12.82	0.141
0.65	29	15.86	0.132
0.85	48	19.97	0.126
0.95	47	22.22	0.122
1.05	52	21.63	0.124
1.15	68	26.34	0.118
1.25	82	26.97	0.111
East Dock site, 1980			
0.20	17	8.23	0.168
0.40	20	8.71	0.160
0.60	22	9.93	0.140
0.80	25	16.63	0.127
1.00	39	17.92	0.131
1.20	56	21.51	0.116

Linear correlation: All data, $r^2 = 0.922$, $a = 6.97$, $b = 0.2726$.

Exponential correlation:

$v_e = 0\text{–}30‰$, $r^2 = 0.703$, $a = 3.347$, $b = 0.0597$

$v_e = 30\text{–}100‰$, $r^2 = 0.926$, $a = 13.09$, $b = 0.0094$

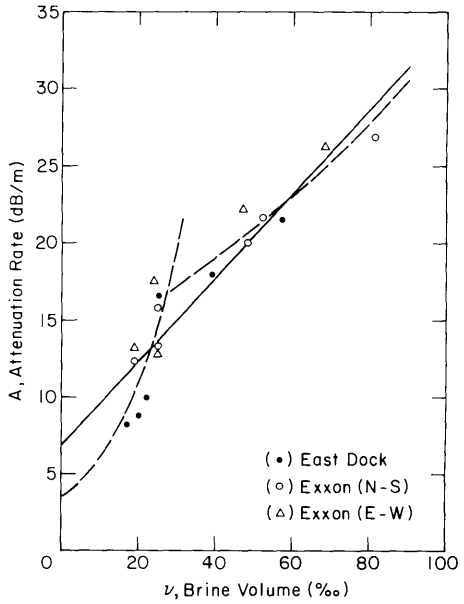

Figure 37. Attenuation rate as a function of brine volume calculated at 100 MHz.

DISCUSSION AND CONCLUSIONS

Time-domain spectroscopy techniques were discussed and measurements presented to determine the complex dielectric constant of sea ice. The object is to understand better the electromagnetic (EM) properties of sea ice as a function of depth in the ice and to correlate these properties with the physical properties of the ice, such as temperature, brine volume, and structure. Several measurement methods were investigated involving the design of EM cells or transmission lines that would minimize the effect of the presence of the EM measuring device on the natural, in situ state of the sea ice.

A simple laboratory model of anisotropic sea ice was constructed from paraffin sheets separated by brine-saturated filter paper. This parallel-plate model of sea ice, when placed in our EM cell, reproduced the polarizing effect noted during field measurement of the bulk EM properties of sea ice. Similar EM cell measurements were made on natural sea ice samples where the azimuthal orientation of the cell's electric (E) field was varied in relation to the preferred horizontal orientation of the *c*-axes of the ice sample crystals.

When the E field was parallel to the preferred horizontal sea ice crystal *c*-axis orientation, the presence of the sea ice sample in the cell produced a minimum change in the signal reflected from the cell, much as with the paraffin-filter paper model. When the cell E field was rotated to be perpendicular to the preferred horizontal crystal *c*-axis alignment there was a significant decrease in the reflected signal, again similar to the paraffin-filter paper model. This demonstrates that anisotropic sea ice can be modeled as a parallel plate structure. It was also found that the anisotropy or polarizing properties of sea ice increase with depth, as does the brine volume.

Two-wire transmission line measurements were made on sea ice samples and in situ. The most informative configuration was a ladder array around which natural sea ice grew. Each step of the ladder was a probe elevation comprised of two parallel lines. Both time-domain transmission and reflection measurements were made as a function of probe depth, for the first time providing information on the in situ dielectric properties and DC conductivity of sea ice vs depth and brine volume. Significant results include:

1. The effect of temperature on brine inclusion conductivity was shown to increase with decreasing temperature down to about $-8^{\circ}C$, at which point the conductivity decreases with decreasing temperature. The latter is probably due to a reduction of ionic mobility in the brine caused by the lower temperature and high ion concentration. There are also less ions available to conduct current because they have recombined to form solid salt crystals.

2. A linear relationship was found between the DC conductivity and the brine volume of the sea ice. As expected, the conductivity was found to increase with increasing brine volume.

3. A description of sea ice as having a formation factor dependent upon porosity (brine volume) and shape of the brine inclusions as formulated by Archie's rule was presented. This relationship now allows one to estimate the DC conductivity of sea ice from the brine volume, which is calculated from the traditional salinity and temperature measurements made on sea ice.

4. An exponential relationship was found between the in situ DC conductivity and temperature of sea ice. Since the brine volume in sea ice is temperature-dependent, the finding that DC conductivity increases with increasing temperature was expected. The interesting result, however, was the sharp break at $-2.2^{\circ}C$ in the conductivity-vs-temperature curve. This inflection point, of marked DC conductivity increase, is believed to be the depth at which EM radar sounding reflections occur near the bottom of first-year sea ice.

5. The estimated depolarization factor for sea ice as a function of depth and the implication this has for the shape and orientation of the sea ice microstructure were discussed. In general, the time-domain spectroscopy measurements indicate that the brine inclusions are arrayed so as to appear tilted from the vertical at an angle of about $45^{\circ} \pm 10^{\circ}$.

6. The complex dielectric constant of sea ice was shown to be a function of the brine volume and the brine-filled microstructure. The real part of the complex dielectric constant was found to be strongly dependent upon brine volume but less dependent upon orientation of the brine inclusions or upon the depolarization factor. In contrast, the imaginary part of the complex dielectric constant was found to be strongly dependent upon brine inclusion orientation but much less dependent upon brine volume.

A final point is that while it is possible to define "standard" sea water, it is not reasonable to define standard sea ice. Sea ice is an ever-changing, extremely complex material, which may be considered as a two-phase system of ice and liquid brine, where in the geometrical structure of the brine inclusions and the ice crystals are highly disordered, irregular, and complicated. The physical structure of sea ice is controlled by such factors as the temperature of the ice and the current velocity and orientation at the ice/water interface. The electromagnetic properties of sea ice are dependent upon frequency, temperature, depth, structure, porosity, pore shape, orientation and distribution, brine conductivity, sensing aspect angle, and so forth. At very low frequencies, near DC, a strong relationship appears to exist between sea ice DC conductivity, temperature, and brine volume. The DC conductivity does not appear to be very dependent on the sea ice microstructure. However, at higher frequencies, 100 to 300 MHz in our study, the complex dielectric constant became more dependent upon the apparent shape and orientation of the brine-filled microstructure. Therefore it would appear that only trends in the relationships between the EM properties of natural sea ice and its brine volume and brine inclusion microstructure can be established, i.e. only bounds may be established on the allowed value of ϵ_{rm}.

Future studies of the electromagnetic properties of sea ice should include a more detailed investigation of the sea ice microstructure, that is, the slope, orientation, and distribution of the pores and channels, as well as the volume of brine and gas within the pores. The latter, for example, is expected to have an extremely small effect on the EM properties of natural sea ice due to the very small fractional volume of gas in natural sea ice.

LITERATURE CITED

Archie, G.E. (1942) The electrical resistivity log as an aid in determining some reservoir characteristics. *Transactions of the American Institute of Mechanical Engineers,* **146**: 54-62.

Assur, A. (1960) Composition of sea ice and its tensile strength. USA Cold Regions Research and Engineering Laboratory, Research Report 44. AD 276604.

Bentley, C.R. (1977) Electrical resistivity measurements on the Ross Ice Shelf. *Journal of Glaciology,* **18**(78): 15-35.

Cherepanov, N.V. (1973) Main results of an investigation of the crystal structure of sea ice (in Russian). *Prob. Arktiki Antarktiki,* 41, 43. (English translation by National Technical Information Service, U.S. Department of Commerce, Springfield, Virginia.)

Davis, J.L. (1979) Electrical property measurements of sea ice in situ using a wide-band borehole radar and a time-domain reflectometer. In *Proceedings of the International Workshop on the Remote Estimation of Sea Ice Thickness, St. John's, Newfoundland, Canada.*

Fellner-Feldegg, H.R. (1972) Permeability, permittivity and conductivity measurements with time-domain reflectometry. Hewlett-Packard Company, HP Application Note 153.

Golden, K.M. and S.F. Ackley (1980) Modeling of anisotropic electromagnetic reflection from sea ice. USA Cold Regions Research and Engineering Laboratory, CRREL Report 80-23. ADA 094620.

Jackson, P.D., D. Taylor Smith, and P.N. Stanford (1978) Resistivity-porosity-particle shape relationships for marine sands. *Geophysics,* **43**: 1250-1268.

King, R.W.P. and G.S. Smith (1981) *Antennas in Matter.* Cambridge, Mass.: MIT Press.

Kovacs, A. and R.M. Morey (1978) Radar anisotropy of sea ice due to preferred azimuthal orientation of the horizontal *c*-axes of ice crystals. *Journal of Geophysical Research,* **83**(12): 171-201.

Kovacs, A. and R.M. Morey (1979) Anisotropic properties of sea ice in the 50- to 150-MHz range. *Journal of Geophysical Research,* **84**(C9): 5749-5759.

Kovacs, A. and R.M. Morey (1980) Investigations of sea ice anisotropy, electromagnetic properties, strength, and under-ice current orientation. USA Cold Regions Research and Engineering Laboratory, CRREL Report 80-20. ADA 092089.

Kraichman, M.B. (1976) *Handbook of Electromagnetic Propagation in Conducting Media.* Naval Materiel Command, NAVMAT P-2303.

Niedrauer, T.M. and S. Martin (1979) An experimental study of brine drainage and convection in young sea ice. *Journal of Geophysical Research,* **84**(C3): 1176-1186.

Reimnitz, E., E. Kempema and C.R. Ross (1982) Observations on the mode and rate of decay of an artificial ice island in the Alaska Beaufort Sea. *Proceedings of 14th Annual Offshore Technology Conference, Houston, Texas,* OTC 4310, pp. 121-132.

Peyton, H.R. (1966) Sea ice strength. University of Alaska, Fairbanks, Report UAG R-182.

Sen, P.N., C. Scala and M.H. Cohen (1981) A self-similar model for sedimentary rocks with application to the dielectric constant of fused glass beads. *Geophysics,* **46**(5): 781-795.

Stogryn, A. (1971) Equations for calculating the dielectric constant of saline water. *IEEE Transactions on Microwave Theory and Techniques,* **19**(8): 733-736.

Taylor, L.S. (1965) Dielectric properties of mixtures. *IEEE Transactions on Antennae and Propagation,* **13**(6): 943.

Tinga, W.R., W.A.G. Voss and D.F. Blossey (1973) Generalized approach to multiphase dielectric mixture theory. *Journal of Applied Physics,* **44**(9): 3897-3902.

van Gemert, M.J.C. (1973) High frequency time-domain methods in dielectric spectroscopy. Phillips Research Reports, **28**.

Vant, M.R., R.O. Ramseier and V. Makios (1978) The complex-dielectric constant of sea ice at frequencies in the range 0.1-40 GHz. *Journal of Applied Physics,* **49**(3): 1264-1280.

Walford, M.E.R. (1968) Field measurements of dielectric absorption in Antarctic ice and snow at very high frequencies. *Journal of Glaciology,* **7**(49):89-94.

Weeks, W.F. and A.J. Gow (1978) Preferred crystal orientations in the fast ice along the margins of the Arctic Ocean. *Journal of Geophysical Research,* **83**(C10): 5105-5121.
Weeks, W.F. and A.J. Gow (1979) Crystal alignments in the fast ice of arctic Alaska. USA Cold Regions Research and Engineering Laboratory, CRREL Report 79-22. ADA 077188.
Wheeler, H.A. (1980) Transmission-line conductors of various cross sections. *IEEE Transactions on Microwave Theory and Techniques,* **MTT-28**(2): 73-83.